Journal of
Marine Science and Engineering

MDPI

Article

Contourite and Turbidite Features in the Middle Caspian Sea and Their Connection to Geohazards Derived from High-Resolution Seismic Data

Vsevolod Yutsis [1,*], Oleg Levchenko [2] and Victoria Putans [2]

[1] División de Geociencias Aplicadas, Instituto Potosino de Investigación Científica y Tecnológica (IPICYT), Camino a la Presa San José 2055, Lomas 4ª Sección, San Luis Potosí 78216, S.L.P., Mexico
[2] Shirshov Institute of Oceanology, Russian Academy of Sciences, 36, Nakhimovsky Prospect, 117997 Moscow, Russia; olevses@gmail.com (O.L.); vitapu@mail.ru (V.P.)
* Correspondence: vsevolod.yutsis@ipicyt.edu.mx; Tel.: +52-444-834-2000

Abstract: High fluvial input combined with specific topographic and oceanographic settings in the Caspian Sea create favorable conditions for contourite deposition. For the first time in its middle portion, contourite deposits have been observed in high-resolution seismic profiles. Various types of contourite drifts and mixed depositional systems have been revealed on the lower slope and in the adjacent basin, some of which are accompanied by sediment wave fields. The deposition of contourites or turbidites and their lateral distribution is controlled by sea-floor topography and oceanographic processes, as well as the modern activity of gravity flows downslope on the western Caucasian slope and in the channel system on the Mangyshlak Sill. The contourite drifts and sediment wave fields form several contourite depositional systems, which seem to merge in the Caspian contourite depositional complex. This occurs near the foot of slopes of the Derbent Basin and is related to the counterclockwise circum-Caspian current in the Middle Caspian Sea. The fact that the Caspian Sea is the largest lake in the world makes this region a significant area for research into the "lake contourites" issue. The Caspian Sea is an important oil-producing area, and sedimentary processes related to the contourite and turbidite can be a source of potential geohazards in the construction and exploitation of underwater engineering structures

Keywords: contourites; drift; sediment waves; bottom currents; turbidite; geohazards; high-resolution seismic data

Citation: Yutsis, V.; Levchenko, O.; Putans, V. Contourite and Turbidite Features in the Middle Caspian Sea and Their Connection to Geohazards Derived from High-Resolution Seismic Data. *J. Mar. Sci. Eng.* **2022**, *10*, 990. https://doi.org/10.3390/jmse10070990

Academic Editors: Assimina Antonarakou, George Kontakiotis and Dmitry A. Ruban

Received: 3 June 2022
Accepted: 12 July 2022
Published: 20 July 2022

1. Introduction

Contourites are deposits of bottom thermohaline-driven geostrophic contour currents [1–3]. Numerous studies in recent years have revealed their presence in a wide range of settings, such as the open ocean, along continental margins, in seas and even in lakes. Despite their apparent abundance, many aspects with respect to the formation, internal structure, and sedimentology of contourites still remain poorly understood in general. The most progress in understanding contourite deposits has been made by studies in deep-water environments, whereas shallow water contourites, including lacustrine contourites, are still largely unknown.

The Caspian Sea (CS) is the largest lake of the world (Figure 1), although it is composed of salt water. The maximum water depth in the Middle Caspian is approximately 700 m. The specific topographic and oceanographic settings of the sea, as well as its high fluvial input, are favorable conditions for contourite deposition; however, bottom circulation and its impact on sedimentation and the sea floor topography in the Caspian Sea still requires further investigation, and appropriate special sedimentological studies for contourite identification in the Caspian have not been carried out. The Caspian Sea is one of the oldest gas- and oil-producing areas, with some sedimentary processes related to the contourites

and turbidites perhaps being sources of potential geohazards in the construction and exploitation of underwater engineering structures. The downslope gravity and turbidity flows causing seafloor erosion and intensive sediment input are treacherous processes for submarine pipelines that could cause pipe rupture, while sediment waves should serve as a warning.

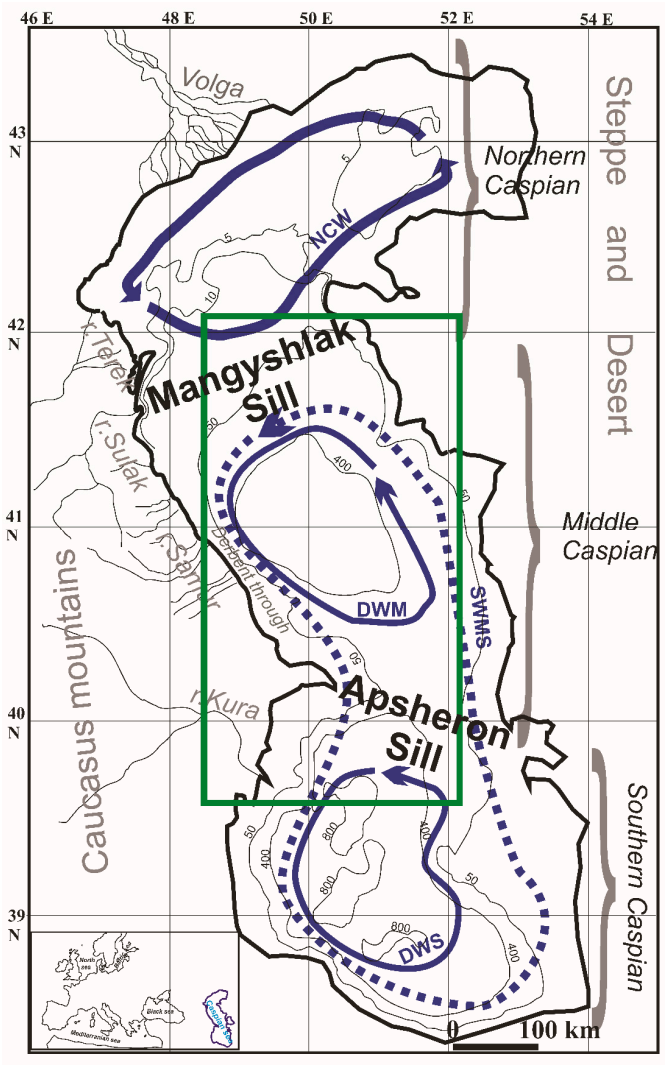

Figure 1. Bathymetric map (m) of the Caspian Sea with regional divisions (northern, middle, and southern) and major geographical sites (mountains, rivers, and steppe). Major bottom currents: NCW (north CS water mass which takes all water levels), SWMS (surface-water mass of the middle and south Caspian sub-basins), DWM (deep water mass of the middle Caspian sub-basin), DWS (deep-water mass of south Caspian sub-basin); river system of the Caucasus Mountains in the west and the Volga River delta in the north are shown. Rectangle shows the area of seismic surveys performed between 2004 and 2012.

Lacustres contourite drift studies could be used to better understand all current-controlled sedimentation processes. Current-controlled sedimentary features have been discovered in Lake Superior (USA), some of the larger West-African Rift lakes, Lake Lago Cardiel (Argentina) and others. For the first time, lacustrine contourite drifts with dimensions comparable to those of their deep-water counterparts were discovered in Lake Baikal (Russia) over an intra-basin high; however, they do not occur in the deep basin or along its margins [4]. Current-controlled sedimentary features in the Caspian Sea are generally located in the lower part of the continental slope and in a deep basin at its foot, which is in keeping with such deep-water features. The morphology and dimensions of

these Caspian Sea features are also comparable to those of many of their oceanic deep-water counterparts. This general similarity may be explained by the fact that some features that are particular to oceans remain in the evolution of the closed Caspian Sea. Nevertheless, giant contourite drifts and fields of sedimentary waves, such as those in the Argentine Basin, have not been found in the Caspian Sea.

The initial recognition of contourite deposits in the marine setting is generally based on reflection seismic data, which is now considered a standard method in most contourite studies. This study is based on a new dataset of mostly high-resolution (HR) and ultra-high-resolution (UHR) seismic reflection profiles collected respectively with the sparker and the parametric sub-bottom profiler SES by the Shirshov Institute of Oceanology in the Caspian Sea between 2004 and 2012 (Figure 2). The results obtained significantly clarified our understanding of the structure of the upper Pliocene-Quaternary sedimentary strata. It was these new data that made it possible to identify, for the first time, accumulative and erosive features in the Middle Caspian, similar to contourite ones [5–8]. This paper focuses on the description of the most prominent erosive and accumulative forms of bottom relief and the Late Cenozoic sedimentary cover of the Derbent Basin (DB) in the Middle Caspian Sea, as well as the processes responsible for the interaction of three different processes. Apsheron Sill (AS) with the along-slope bottom contour currents, the formation of the Late Cenozoic sedimentary cover is affected by the downslope turbidite and gravity flows.

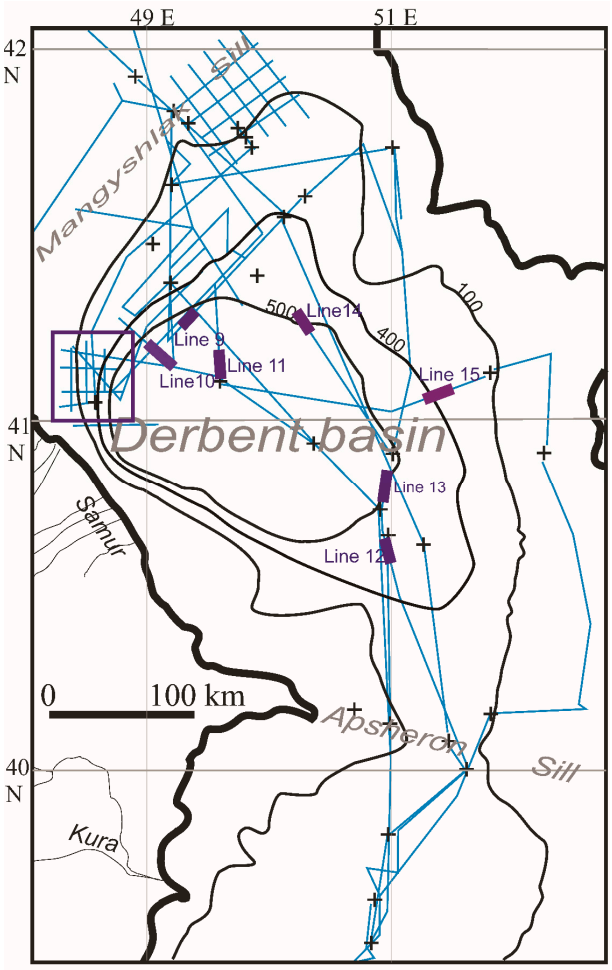

Figure 2. Scheme of seismic reflection profiles (high (sparker) and ultra-high (SES) resolution), collected by Shirshov Institute of Oceanology from 2004 to 2012. The straight lines show the positions of the seismic profiles illustrated in Figures 3–15. The rectangle shows the position of the seismic profiles shown in Figure 4. Crosses for oceanology stations.

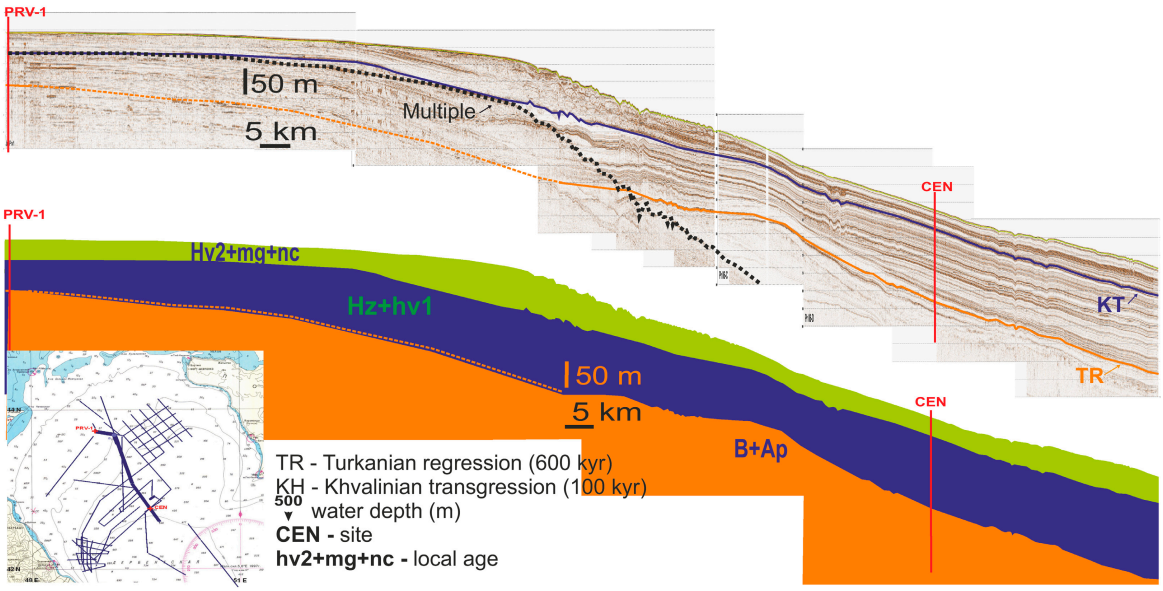

Figure 3. Middle Caspian sparker data and stratigraphy scheme. Regional unconformities: TR—Turkanian regression (600 kyr), KH—Khvalinian transgression (100 kyr). Local age: B + Ap—Bakinian and Apsheron transgressions, Hz+Hv1—Khazar and Khvalinian (first step) transgressions, hv2 + mg + nc—Khvalinian (second step) transgression, Mangyshlak regression (7–10 kyr) and new-Caspian transgression. CEN—Site Centralnaya. PRV-1—Site PRV-1.

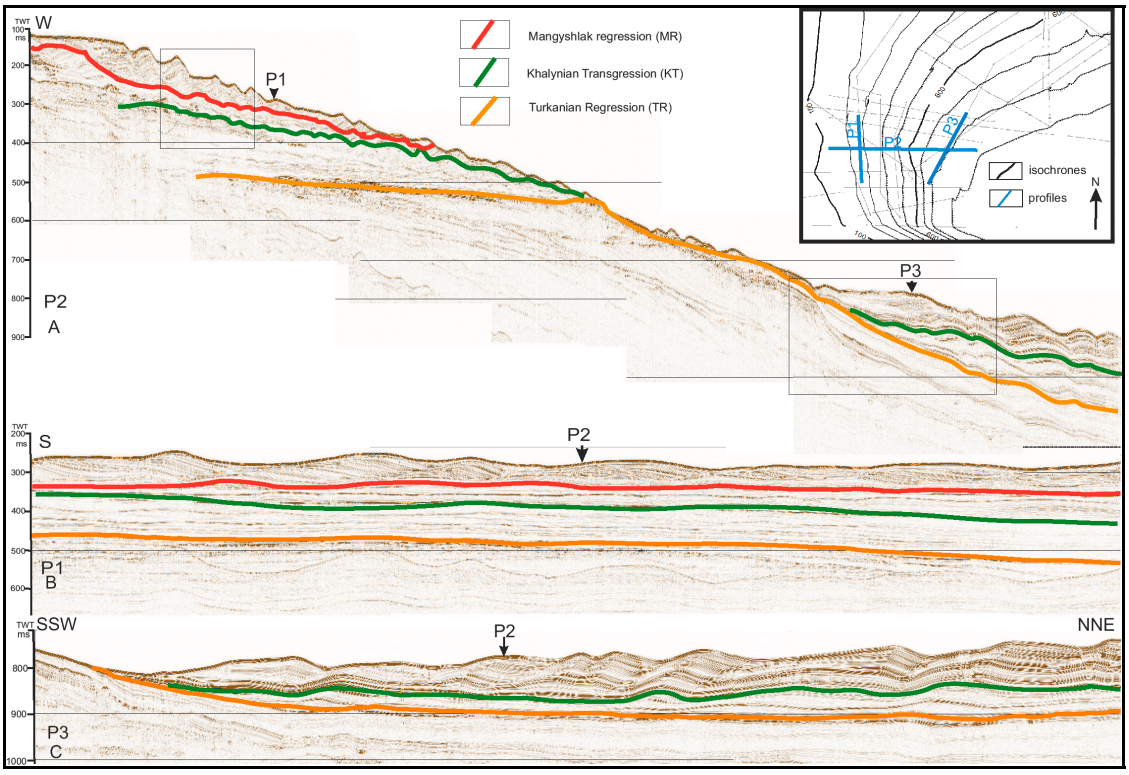

Figure 4. High resolution seismic profiles (sparker) on the western slope of the Derbent Basin off the Caucasus Mountains. (**A**) P2—Seismic profile P2, W-E across the slope; (**B**) P1—Seismic profile P1, S-N along the slope; (**C**) P3—Seismic profile P3, SW-NE along foot of the slope. Location in inset. The rectangle at the top left of Figure 4A shows a fragment of this seismic profile, illustrated in detail in Figure 5. The rectangle at the bottom right of Figure 4A shows a fragment of this seismic profile, illustrated in detail in Figure 6.

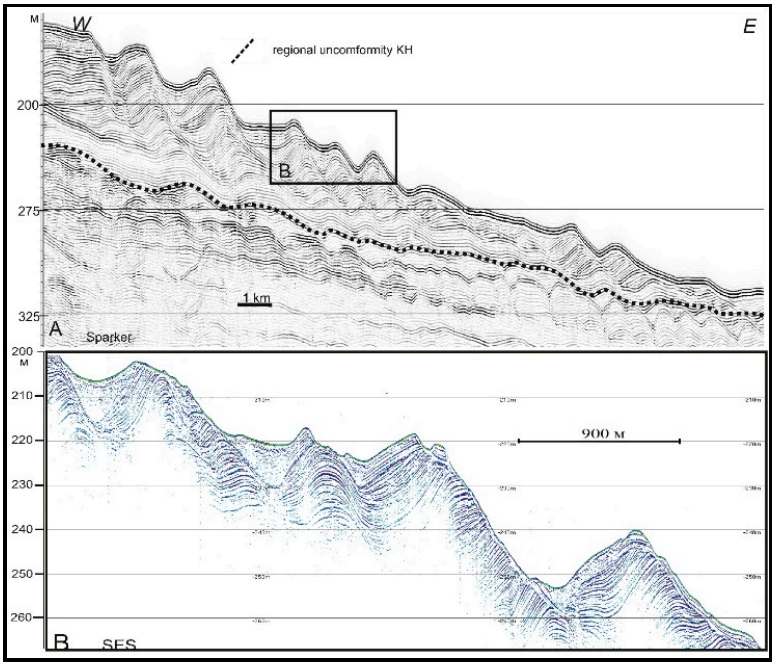

Figure 5. Sediment waves of turbidity + contourite genesis on the western slope of the Derbent Basin. (**A**) Fragment of the profile (sparker) from Figure 4A. KT—regional unconformity Khvalinian transgression. (**B**) Enlarged fragment of ultra-high-resolution seismic reflection profile (SES) showing in detail uppermost sedimentary layer with evidence of the young to present-day erosion activity.

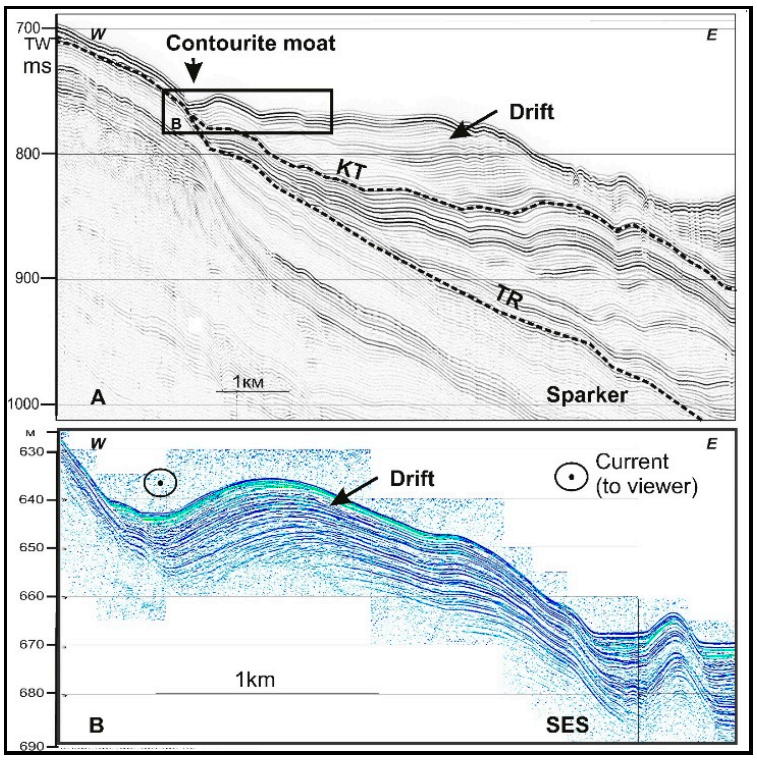

Figure 6. Separated drift in the contourite mounded elongate drift at the foot of the western slope of the Derbent Basin. (**A**) Fragment of the profile (sparker) from Figure 4A. Main unconformities: TR –Turkanian regression, KT—Khvalinian transgression. (**B**) Enlarged fragment of ultra-high-resolution seismic reflection profile (SES) showing in detail uppermost sedimentary layer with a migration drift dome and adjacent erosional moat. Current in moat is to the viewer.

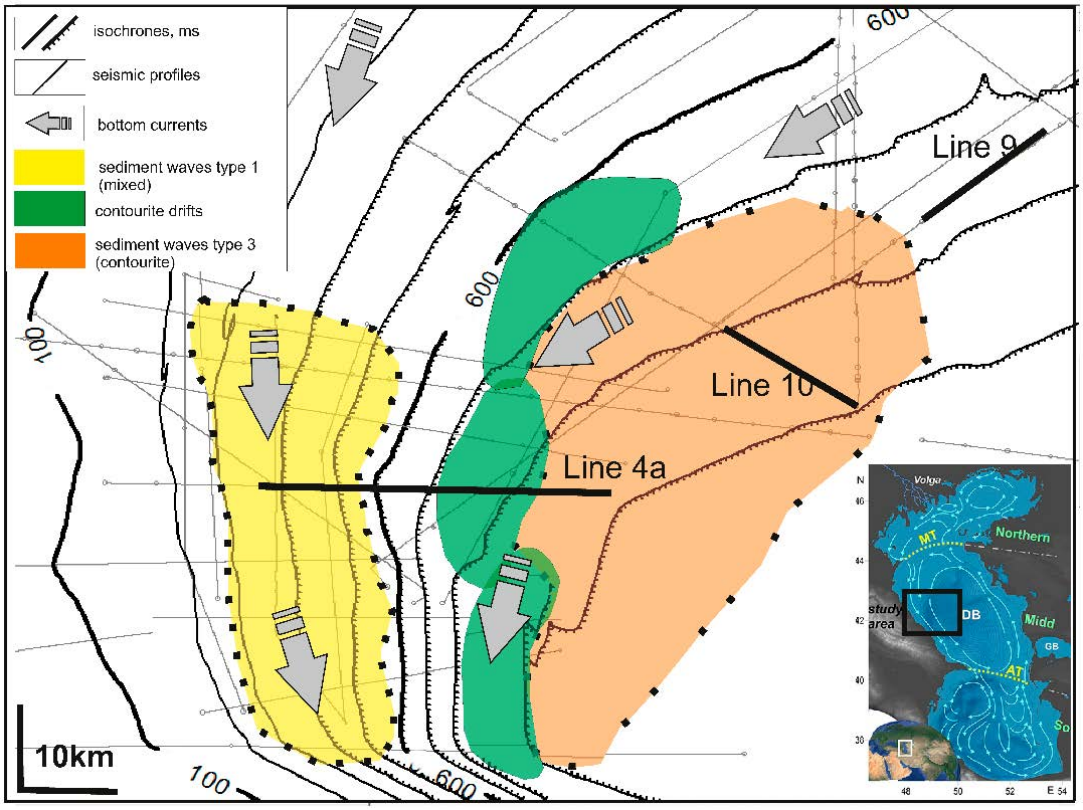

Figure 7. Contourite deposits near the western slope of the Middle Caspian Sea. Location in insert. Arrows for near bottom water currents. Lines 4a, 9, and 10 show the positions of the seismic profiles shown in the corresponding figures.

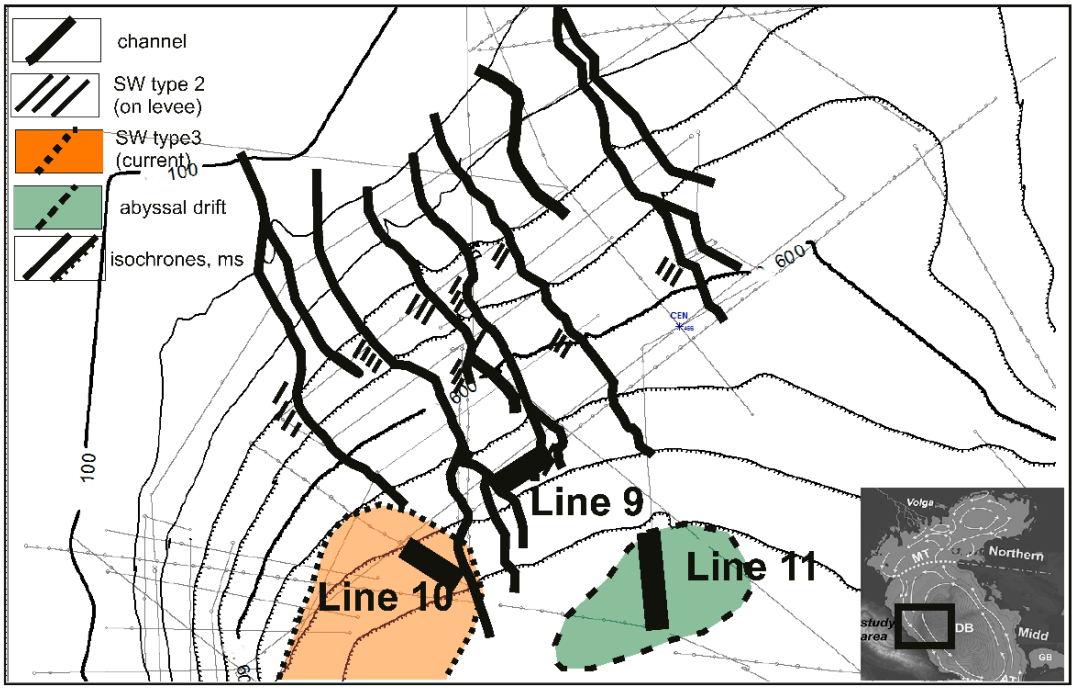

Figure 8. Scheme of modern channel system over the Mangyshlak Sill and contourites off the northern slope of the Middle Caspian Sea: sediment wave types 2 (on levee) and 3 (contourite) and abyssal drift. Lines 9, 10 and 11 show the positions of the seismic profiles shown in the corresponding figures.

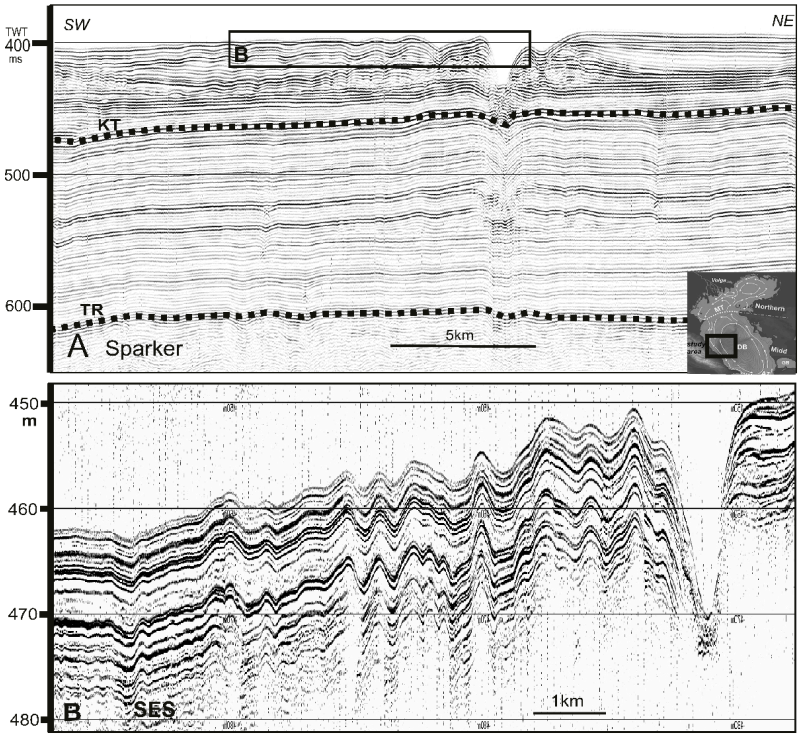

Figure 9. Sediment waves type 2 (on channel levees) on the northern slope of the Derbent Basin near the Mangyshlak Sill. (**A**) Fragment of the profile (sparker) SW-NE trending along foot of the slope. Main unconformities: TR—Turkanian regression, KT—Khvalinian transgression. (**B**) Enlarged fragment of ultra–high-resolution seismic reflection profile (SES) showing in detail uppermost sedimentary layer. Location of the profiles is shown in Figures 2 and 8.

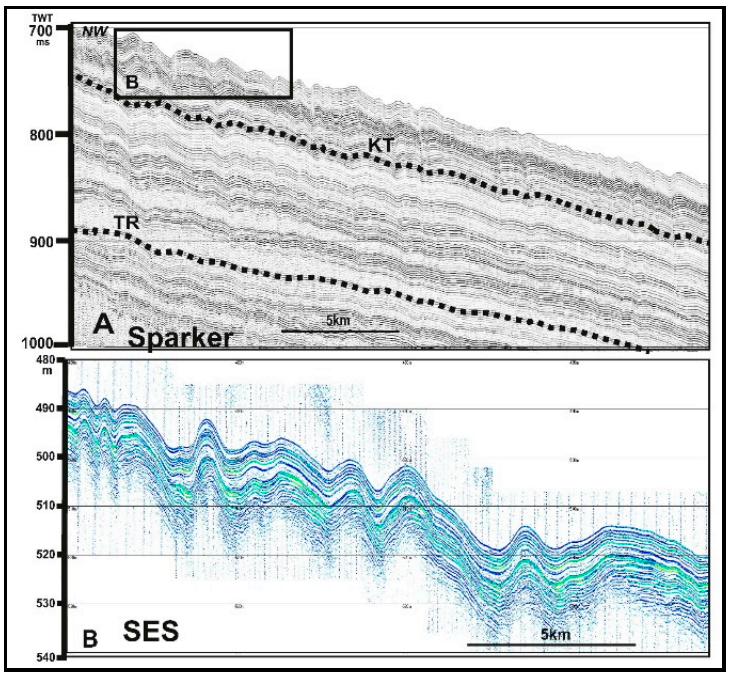

Figure 10. Sediment waves type 3 (contourite) on the northern slope of the Derbent Basin near the Mangyshlak Sill. (**A**) Fragment of the profile (sparker) NW-SE trending across foot of the slope. Main unconformities: TR—Turkanian regression, KT—Khvalinian transgression. (**B**) Enlarged fragment of ultra-high-resolution seismic reflection profile (SES) showing in detail uppermost sedimentary layer. Location of the profiles is shown in Figures 2 and 8.

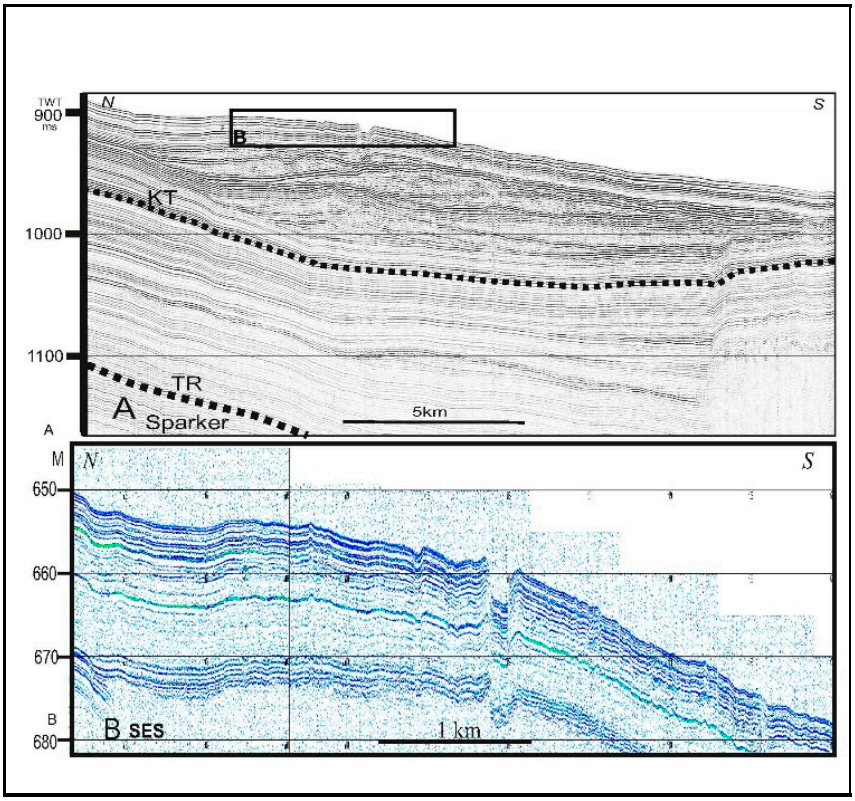

Figure 11. Contourite detached drift in the northern Derbent Basin off the Mangyshlak Sill. (**A**) Fragment of the profile (sparker) NW-SE across foot of the northern slope. Main unconformities: TR—Turkanian regression, KT—Khvalinian transgression. (**B**) Enlarged fragment of ultra-high-resolution seismic reflection profile (SES) showing in detail uppermost sedimentary layer with present-day channel. Location in Figures 2 and 8.

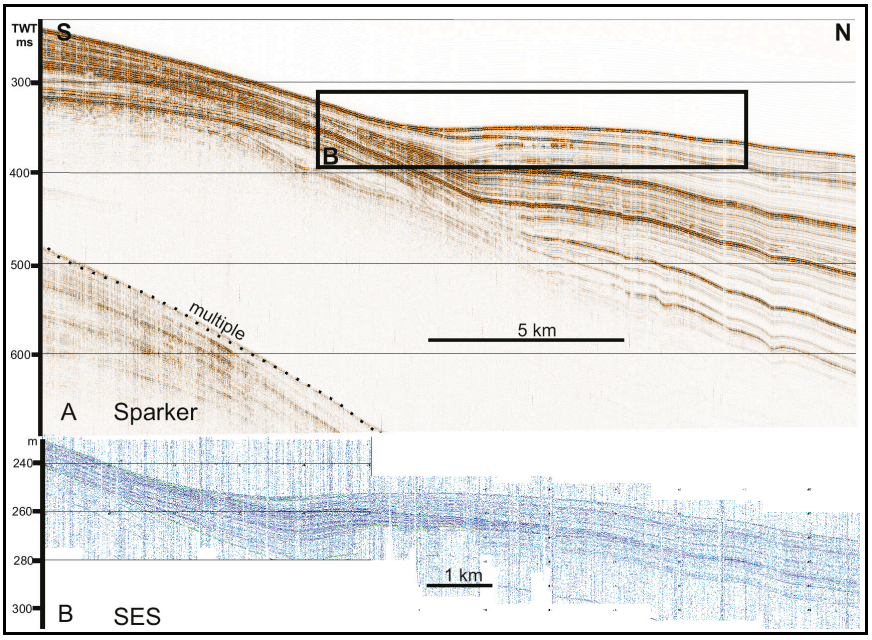

Figure 12. Contourite plastered drift on the southern slope of the Derbent Basin near the Apsheron Sill. Fragment of the profile (sparker) roughly S-N across the slope. (**A**) Fragment of the profile (sparker). (**B**) Enlarged fragment of ultra-high-resolution seismic reflection profile (SES) showing in detail uppermost sedimentary layer. Location in Figure 2.

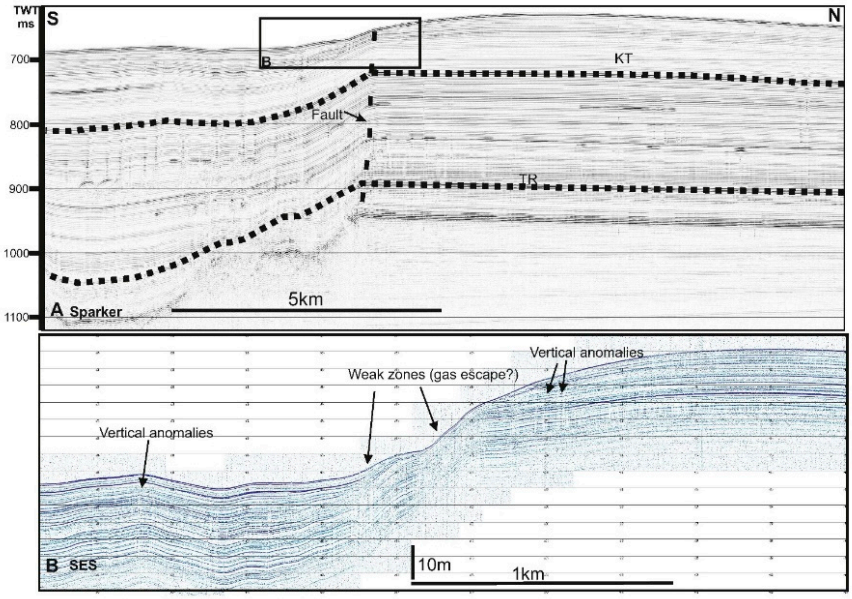

Figure 13. Contourite fault-controlled drift on the southern slope of the Derbent Basin near the Apsheron Sill. (**A**) Fragment of the profile (sparker) roughly S-N along foot of the slope. Main unconformities: TR—Turkanian regression, KT—Khvalinian transgression. (**B**) Enlarged fragment of ultra-high-resolution seismic reflection profile (SES) showing in detail uppermost sedimentary layer with weak acoustical transparent gas escape zones. Location in Figure 2.

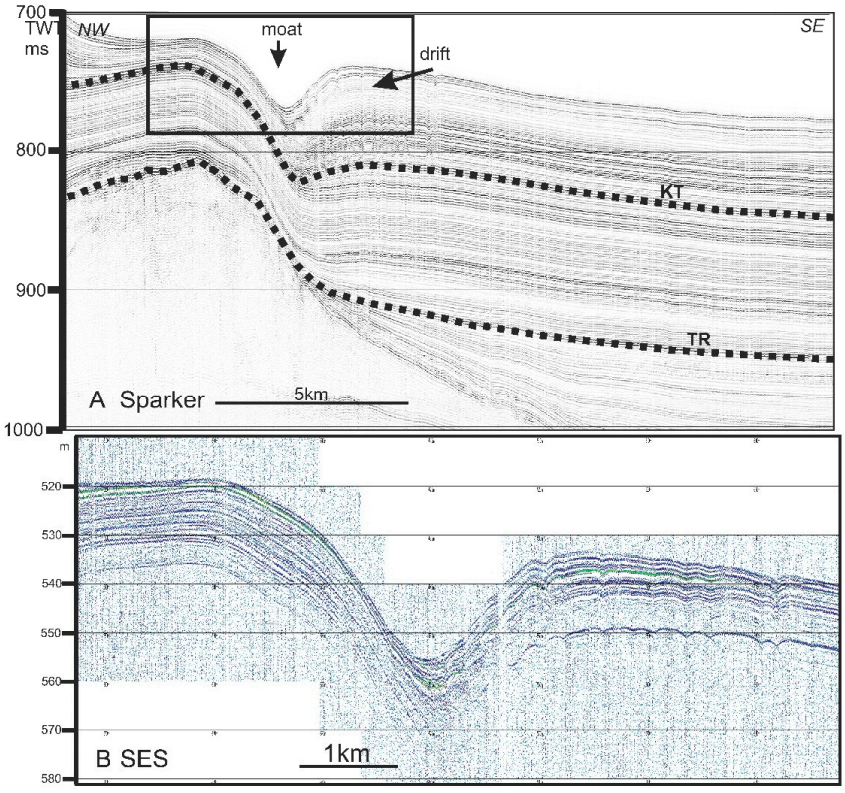

Figure 14. Contourite separated drift and deep erosional moat in the Derbent Basin off its eastern slope. (**A**) Fragment of the profile (sparker) NW-SE along foot of the slope which shows buried ancient creep deformation. Main unconformities: TR—Turkanian regression, KT—Khvalinian transgression. (**B**) Enlarged fragment of ultra-high-resolution seismic reflection profile (SES) showing in detail uppermost sedimentary layer with lens of the drift. Location in Figure 2.

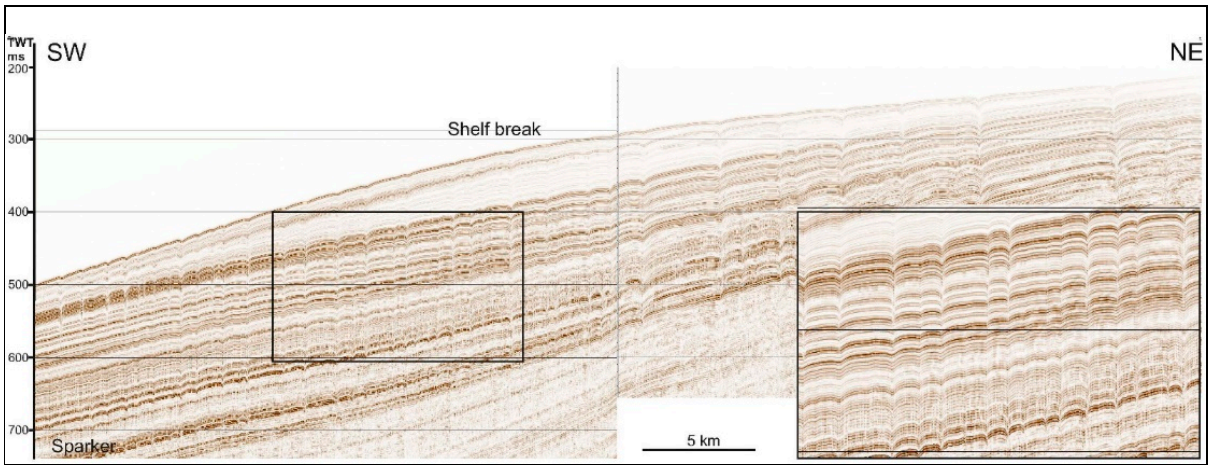

Figure 15. Exogenic–gravitational folds or creep deformation on the eastern slope of the Derbent Basin. Fragment of the profile (sparker) SW-NE trending across foot of the slope. Location of the piles is shown in Figure 2.

High regional seismicity initiates numerous landslides and density flows on the slopes of the Derbent Basin. The exogenic–gravitational folds in the Quaternary clayey and calcareous–clayey sediments were previously defined along the eastern slope of the Derbent Basin, which were produced by the plastic flow of poorly consolidated sediments under the influence of gravitational forces [9]. Our HR and UHR surveys revealed similar slump box-shaped rootless folds on the northern slope of the Derbent Basin [10]. These new seismic reflection data made it possible to reveal the structure of the upper sedimentary layer of the western slope of the Derbent Basin in greater detail. Areas with a chaotic pattern of the acoustic record are marked here, which are interpreted as a set of separate slump and landslide blocks [11]. They appear to have moved in the recent geologic past (Late Quaternary) down a relatively steep slope. These landslide deformations and gravitational features were previously considered [10,11]; therefore, in this paper, we focus on the description of turbidite features and, mostly, contourite ones.

This paper focuses on the bottom and sub-bottom features in the central part of the Caspian Sea (the Middle Caspian) and the processes of near bottom water circulation which formed these features. Our main objectives are (1) to test the contourite paradigm on special sea-lake conditions, where the morphology is similar to an oceanic one, but all oceanography processes occur in far smaller time-space scale, and (2) to explore potential geohazards of which contouritic features can be signs.

2. Regional Settings

The Caspian Sea (CS) is located between Europe and Asia and is the largest lake in the world; however, its physical environment and its floor have mixed oceanic-continental characteristics [12]. The CS was created tectonically when the Paratethys began splitting into smaller water bodies some 5.6 million years ago [13]. Now the sea is confined between the Caucasus Mountains in the south and west, the vast steppe of Central Asia in the east and an extensive alluvial plain in the north (Figure 1). The water surface is almost 28 m below the World Ocean level [14]. The sea extends for about 1030 km from north to south and for 196–433 km in the east-west direction (total area 386,400 km^2 in 2017 [15]).

2.1. Geological Setting

The Caspian Sea is divided into three parts (Figure 1): northern, middle, and southern [16]. The northern part is the shallowest with a maximum depth of 25 m and smooth bottom topography. The Middle Caspian Sea represents a large depression separated from the northern and southern parts by the Mangyshlak Sill (a bow-shaped depositional body) and the Apsheron Sill (a large structural high), respectively. A major part of the Middle

Caspian area is occupied by the Derbent Basin, which is contoured by an isobath of 400 m and has a maximum depth of 788 m. The Southern Caspian Basin is the deepest part of the sea, with a maximum depth of 1025 m [17].

The seismotectonic provinces were mapped by Ivanova and Trifonov [18] using the criteria of Earth's crustal structure, specific features of neotectonic (Pliocene–Quaternary) evolution, the pattern and kinematics of active faults, as well as the distribution of earthquake focal zones and the dynamics of their activation during the last 160 years. Average seismic energy values were computed for individual seismotectonic provinces that differ in the Earth's crustal structure as regards the intensity of neotectonic movements and seismicity. Our study concerns an area of contrasting combination of the Caucasus Mountains with the Derbent Trough in the west of the Middle Caspian region (Figure 1). The structures originated simultaneously in the Pliocene–Quaternary, and their formation was accompanied by a reworking of the Earth's crust in the post-Paleozoic era [19]. The main earthquake focal zone, which features events of up to M = 6.3 with hypocenter depths of up to 110 km, extends along the southwestern slope of the Derbent Trough. Significant geological processes on a regional scale are neotectonic movements and deep-focus earthquakes. Seismicity triggers mud volcano activity and mass movements on the slopes of both deep basins in the Middle and Southern Caspian.

The western slope of the Derbent Basin is characterized by a slope angle from 0° to 4° and a "double break" at water depths of 100 m and 400 m (Figure 3). The upper break correlates with isobath 100 m and marks the outer edge of the modern shelf; the lower break goes with isobath 400 m, which outlines the Derbent Basin. The Mangyshlak Sill and the northern slope of the Derbent Basin are intersected by a channel system, which relates to the overall fan of the Volga, Terek, and Ural rivers.

The Caspian Sea's most unique feature is the unpredictable and fast level changes, which are impossible to correlate either with the World Ocean or with the history of glaciations [20,21]. Furthermore, seismicity variations for the Caspian region do not point to any unique correlation with the sea level oscillations. At the same time, tectonic processes, which are partly reflected in seismicity, make a significant contribution to the contemporary CS level oscillations [18]. This manifests itself in sea level rises during large earthquakes and, more convincingly in a correlation between values of the total seismic energy released in individual seismotectonic provinces in the region and sea level changes. The tectonic impacts produce an integral effect of interaction between the deformation processes, causing changes in the sea basin volume (depression deepening or transverse shortening, and local anticline growths), which may be supplemented by an intermittent water supply from the deep-seated layers of the sedimentary cover [22]. This supply could be more significant in the deep and rapidly subsiding South Caspian depression, where it is enhanced by faults revived by earthquakes [18]. Since 2016, the CS level seems to have stabilized to an equilibrium at −28 m [14]. As it is an endorheic lake, CS level variations are mostly controlled by water discharge from rivers, direct precipitation and evaporation over the CS [14,23].

The Caspian deep-water environment benefited from the water-level fall until 2016 and the consequent accelerated circulation that causes deep-water ventilation and nutrient exchange; however, most changes are felt at the surface level [14].

2.2. Sedimentation Setting

The maximum thickness of sediments in the Derbent Trough is 14 km, while the thickness of Pliocene–Quaternary sediments is >5 km. It should be noted that the most intense subsidence only began at the end of the Pliocene and is continuing at the present time, remaining uncompensated by sediment accumulation [19,24].

Sedimentation processes in the Caspian Sea are controlled by bottom topography and sources of sedimentary material (river runoff first), as the Caspian Sea is asymmetric in terms of sediment input. Its western part is dominated by a strong alluvial input: a slope adjoins the high chain of the Great Caucasus Mountains with many mountain rivers,

most notably, The Terek, Sulak, Samur and Kura. Runoff sediments move across the shelf and down the western slope; nevertheless, the highest surface concentration suspensions (41 mg/L) are measured on the northern Caspian and in the delta of the Volga River [16]. The overall sediment discharge of more than 130 rivers exceeds 110 tons per year [25], while the eastern part of the sea is adjacent to the desert and is characterized by the absence of river input and a prevalence of aeolian processes [26].

2.3. Hydrological Settings

The differences in water masses, which are mainly created by the climate, lead to relatively distinctive physical and chemical specifications. To a lesser extent, geological forces may cause a mixing of water masses, e.g., by the dispensing of materials and energy through the water column. Four flows of water masses circulation seem to be identified in the Caspian Sea (Figure 1): (1) the north CS water mass, which takes all water levels (NCW), (2) the surface-water mass of the middle and south Caspian sub-basins (SWMS), (3) the deep-water mass of the middle Caspian sub-basin (DWM) and (4) the deep-water mass of south Caspian sub-basin (DWS) [27]. The Apsheron Sill separates the two deep-water masses of middle and south sub-basins and prevents free mixing between them. The middle Caspian deep-water mass has a lower temperature and salinity and higher dissolved oxygen content, compared to the southern one [14].

Vertical exchange in the middle CS is partially caused by wind forcing that forms a cyclonic gyre in the center and upwelling along the east and west coasts of the middle Caspian sub-basin, which leads to contrasting temperatures. Moreover, the intense evaporation at the eastern coast may cause local saline and dense warm water to penetrate deeper waters [28]. Extensive water exchange among the water masses occurs during the cold season. The winter convection mixes the water column vertically, and during mild winters, it penetrates down to around 200 m in the middle Caspian masses. During severe winters, it reaches down to enable the vertical mixing of oxygen and other biochemical elements [29,30]. The vertical mixing is forced by wind, evaporation and winter convection; this, however, is not affected by current water-level fluctuations. The Arctic-type mixing occurs annually in the CS, and it affects the whole Caspian water mass [17]. The strength of this type of mixing is closely related to the severity of winter and the Caspian water-level status. During water-level lowstand, mixing would be stronger and deeper; however, in the highstand, it would hardly reach deep-water masses.

The rate of the CS deep-water circulation has changed significantly during water-level fluctuations [17,31]. The Middle Caspian Sea is characterized by a counterclockwise circulation of surface currents (Figure 1). Intense current sweeps fine-grain sediments from the northern area down to the Derbent Basin, where abundant mass-wasting deposits form and sometimes cause gravity flow activity. Although deep-water currents are poorly studied there, it is proposed [25,32] that the bottom circulation has the same pattern as the surface circulation; this was proven by recent hydrological and mineralogical studies [26,33], where an active bottom current along the western slope of the Derbent Basin was revealed. Near the eastern slope, surface currents form vortices and water masses sink along with pycnocline at the deep-sea level and the velocity of bottom currents increases up to 1 m/s [33]. Thus, a contour current is flowing along the western slope roughly from NNW to SSE, while along the eastern slope, it is flowing from SSE to NNW. A strong upwelling of cold deep water is observed near the eastern slope [33]. The experimental material shows the seasonal variability of the flow of the cyclonic cycle along the western coast of the Middle Caspian. The observations showed that the cyclonic circulation in the Middle Caspian is, essentially, a seasonal contour current flowing around the slope of the Derbent Depression. In winter (December–February), the current in the circulation is relatively fast (up to 70 cm/s), while in summer (June–August), it practically disappears everywhere, except for its western branch, which carries water into the Southern Caspian [34].

The formation of the bottom current in the Caspian Sea is associated with the Volga River's giant outflow of water into the shallow northern part of the Caspian Sea, and its

paths are determined by the relief of the Middle Caspian Sea bottom. Moving southward, this water rolls into the deep water Derbent Basin, forming a flow along its western slope. This is confirmed by the observed channels in the lower part of the slope and adjacent basin. Furthermore, when reaching the Apsheron Sill, the bottom water flow turns eastward along the southern slope of the Derbent Basin, then turns northward along the eastern slope of the Derbent Basin.

In the open ocean, bottom contour currents are associated with thermohaline circulation created by the difference in water density resulting from the inhomogeneous distribution of temperature and salinity in the ocean. This circulation creates a global ocean conveyor belt in the world's oceans. In the closed Caspian Sea, the formation of the bottom current is associated with the giant Volga River outflow, and the geometry of this bottom current distribution is determined by the topography of the Middle Caspian Seabed.

2.4. Stratigraphy Setting

The stratigraphy of the upper sedimentary sections on the shallow-water shelf and the upper slope areas in the Middle Caspian Sea is determined mostly by regional transgressions and regressions [20]. On long time scales, Caspian Sea level oscillations are dramatic. During the last 8000 years, the sea level has fluctuated repeatedly with amplitudes up to at least 25 m, even dropping from a Last Glacial highstand at +50 m down to possibly −113 m in the early Holocene [35,36]. The causes of Caspian Sea level change are not yet fully understood. Caspian Sea levels depend largely on the balance between the influx of the Volga River water and evaporation over the sea surface [15,37]. However, the correlation of Caspian Sea level with global and regional circulation patterns, which cause precipitation in the Volga basin, is often surprisingly poor, or only significant for specific intervals with relatively stable sea levels [38]. In spite of great advances in understanding of our climate system, the predictive power of our Global Circulation Models, and accurate monitoring by satellite systems, such as Topex-Poseidon/Jason, opinions about future Caspian Sea level trends diverge. Some authors do not believe in climatic forcing at all, referring instead to tectonics, geochemical causes, or chaotic behavior [39].

Previous data interpretation showed three regional acoustic sequences [40]. Due to two deep drilling sites, it was possible to refer the acoustic sequences to lithological ones and to the regional stratigraphic scale and absolute age. Such correlation proves the TR (Turkanian regression) and KT (Khvalinian transgression) horizons to be one of the largest regional stratigraphic markers. These are as follows: TR, the most dramatic Caspian regression in the last 1 million years (occurred about 600–700 kyr ago); and KT, the most dramatic transgression of the whole Caspian history (occurred about 100 kyr ago) (Figure 3). There is also the M horizon, which is correlated to the Mangyshlak regression (10 kyr) (vertical resolution of Figure 3 is not enough to show the MR horizon). For details see Section 4.1 of this paper.

3. Materials and Methods

The study is based on high- and ultra-high-resolution seismic reflection profiles collected by the Shirshov Institute of Oceanology in the Caspian Sea between 2004 and 2012 (Figure 2). The techniques used provide both high resolution and penetration of acoustic signals below the seafloor.

3.1. High-Resolution Seismic Reflection Profiling (Sparker)

The high-resolution (HR) seismic reflection profiling was carried out using a multi-electrode (64–114 pieces) sparker (500–1000 J) towed at a depth of 0.5–1.0 m. The shot interval was set to 1 or 2 s, and the bandwidth of the transmitted seismic signal was 100–1000 Hz. The 25 m long single-channel streamer was towed at water depth of 0.5–1.0 m, with the collected data being visualized in real-time and recorded on a PC in the SEG-Y format with simultaneous processing (initial muting, filtration). More advanced processing of the seismic data was carried out after the field campaign in the RadExPro software

package (more frequency filtering, muting, static correction, equalization of the amplitudes, deconvolution, etc.). Depending on sediments, penetration varied between tens and hundreds of meters with a resolution from a minimum of 2 m. The resulting SEG-Y files were imported into a Kingdom Suite™ project for interpretation.

3.2. Ultra-High-Resolution Parametric Profiling (SES UHR)

The ultra-high-resolution seismic reflection profiling (UHR) was carried out using the two-channel (high-frequency (HF), 100 kHz, and low-frequency (LF), 4–15 kHz) parametric acoustical system SES-2000 standard (Innomar Technology, Germany). The hardware includes an echosounder and sub-bottom profiler, and the HF (100 kHz) channel is used for bathymetric surveying.

Depending on the selected registration mode, the shooting rate can be up to 30 shots per second and depending on the sediments, penetration and resolution, are 50 m and 5 cm, respectively. The motion sensor MRU-H was used to resolve the sea swell. Data were collected and displayed in real time by original software SESWIN. For further processing, the special software ISE 2 was used.

4. Results

The high-resolution seismic reflection surveys revealed expressive erosional and depositional features on slopes and the rise of the Derbent Basin and in the middle part of the Caspian Sea [5,7,41]. These features had not been distinguished earlier as contourites because of the low resolution of air gun seismic profiling, and similar ones were considered here as slump or landslide features, tectonic folds, or creep deformations [9,32]. The high-resolution seismic reflection data presented in this paper were collected mainly in the western part of the Middle Caspian Sea and significantly less in the eastern part (Figure 2).

4.1. Western (Derbent) Slope

The sparker seismic profiles on the western slope of the Derbent Basin show some strong reflectors (Figure 4), which emphasize the complex history of transgressions and regressions in the Caspian Sea [40,42]. The strong sub-horizontal reflector TR (see Section 2.4 of this paper) in the base of the upper sedimentary wedge between edge of the shelf (water depth ~100 m) and sharp bend of the slope (~400–550 m) (Figure 4) correspond to the erosional unconformity formed during the great Turkanian regression of around 700–800 ka, when the sea level dropped by ~180 m. Another strong rough KT reflector (see Section 2.4 of this paper) expresses the dramatic Khvalinian transgression of around 20–30 ka, which was largest during the Quaternary of the Caspian Sea when the sea level rose by ~50 m. The upper non-smoothed strong MR reflector corresponds to the erosional unconformity formed during follow-up the Mangychlak regression about 7–10 ka, when the sea level dropped again by ~60 m [9,32]. Therefore, the sedimentary wedge of its upper part between edge of the shelf (water depth ~100 m) and sharp bend of the slope (~550 m) is composed of sediments from the Middle Pleistocene–Holocene.

The expressive seafloor and subsurface undulating features, which are observed in the high-resolution seismic reflection profiles (Figures 4 and 5), were interpreted as sediment waves [43]. We call them SW Type 1; they are 300–1600 m (on average 1 km) in wavelength across the continental slope and 5–40 m high (on average 20–25 m). The highest amplitudes are observed in the upper slope just behind the shelf edge, and they decrease in a gradual downslope seaward. The angles of the limbs range from some minutes to 3–4°, with the maximum angles being in the upper slope and decreasing downslope. These regularly spaced wave-like accumulative features have steep western coastward limbs and gentle eastern seaward ones. It seems that the top of the accumulative features moves sequentially toward the coastline, with superposed individual layers representing a migrating up slope wave configuration. The detailed bathymetry survey showed that the N–S trending sediment waves are not elongated features, but rather ellipsoid-shaped ones with an axis ratio of 1:3 (like brachyanticlines), which strike along the continental slope [40,42]. These

sediment waves appear to form a vast field covering an area of ~7500 km^2. The ultra-high resolution SES profiles collected show erosion seabed forms (Figure 4B).

At the base of the western slope, at water depths from 450 to 750 m, there is a large accumulative sedimentary body (interpreted as separated drift, see Section 5.2 of this paper) ~70 m thick with uneven internal reflectors (Figure 6A). The upper thin-layered sequence with numerous parallel curved up reflectors conformal to the seabed has a thickness of ~15 m (Figure 6B). On the contrary, the deeper internal reflectors are curved down following the geometry of the main unconformity KT (Figure 6A). This sedimentary accumulative body that extends along the regional contours for about 80 km is subdivided into three depositional mounds (Figure 7), which have almost the same dimensions: 8–11 km in width, 25–30 km in length, and their average length/width ratio is 3:1. All of them are separated from the slope foot by the shallow moat around 1–2 km deep, with their depth increasing southward from 4 to 12 m. Seismic data demonstrate the absence of modern unconsolidated sediments in the moat (Figure 6B).

The profiles show a good range of downslope features. According to previous research [10,11], uplifts in the upper part of the western slope of the Derbent Basin do not represent individual slump bodies moving along the seafloor; nevertheless, the internal structure of the Neopleistocene sequence in this area suggests the presence of numerous intraformational slump duplexes. In the steepest part of the slope, clear indications of the disintegration of bottom deposits and collapsing and slumping processes were revealed. However, an extensive discussion of downslope features here does not fit into the main context; therefore, it would be more appropriate to continue the discussion in another publication.

4.2. Northern Slope (Mangyshlak Sill)

The upper part of the northern slope of the Derbent Basin is called the Mangyshlak Sill. Its main geomorphologic feature is a vast channel system built by the Volga River and some rivers from the Caucasus (Figure 1). The channels run across the slope (Figure 8). The undulated, wave-like acoustic facies that climb toward the channel axes are usually observed on the channel's western flanks (Figure 9A). The dimensions of these wavy features (height and wavelength) decrease laterally from the channel axes (Figure 9B); we have labeled them SW—Type 2.

Relatively deep-water sediment waves are observed in the corner between the northern and western slopes of the Derbent Basin (Figure 10). They are characterized by the absence of migration and very slight and unpredictable downslope decreasing in height (from 10 to 4 m) and wavelength (from 1.7 to 0.5 km). The field of these migrating sediment waves starts at the western slope and ends below the northern one, so it occupies several tens of square kilometers (Figure 7). We have labeled them SW—Type 3.

A large lenticular accumulative sedimentary body (detached drift) is observed in the Derbent Basin near the base of the northern slope at water depths from 670 to 720 m (Figure 11). It is over 30 km long and 15 km wide (length/width ratio 2:1), rising 20 m above the seafloor. The maximum thickness of the body down to the reflector KT is about 100 m. Its visual inner seismic reflection pattern is very complicated with different types of reflections (except conformal horizontal/parallel ones). The thin-layered sequence of parallel smooth reflectors directly below this unconformity KT differs dramatically from the irregular architecture of the overlying deposits. In the bottom relief, the drift is complicated by a channel-looking feature (Figure 11); however, this feature can be interpreted as a crater because canyons are normally V-shaped and have new sedimentation at the bottom, but the materials at the bottom of this structure seem to collapse down. Gerivani et al. [44] interpret this structure as a crater formed by a mechanism such as that suggested and described by [45,46] for "hill-hole pairs". In this crater, it seems that the mixture of high-pressure gas, sediments and water were first emitted from probably weak zones in both sides of the crater, and then the upper beds collapsed down.

4.3. Southern Slope (Apsheron Sill)

Two prominent large accumulative sedimentary bodies are observed on the southern slope the Derbent Basin in the eastern part of the Apsheron Sill. The upward convex lenticular gently sloped depositional body (plastered drift) extends for about 20 km at depths from 250 to 300 m and is related to an erosional moat-like feature with a depth of 10 m and width of around 2 km (Figure 12). The pinching-out upslope of the internal reflectors and local unconformities within thin-layered strata evidence lateral migration of the sedimentary feature.

The second body (interpreted as fault-controlled drift, see Section 5.2 of this paper) observed at a depth range of 470–520 m is interrupted by a fault that significantly changes its overall geometry. The northern part of the fault seismic record is characterized by continuous, parallel, roughly horizontal reflectors, while in the southern part, reflectors demonstrate distinct undulation (Figure 13). The fault influence is a syn-fault sedimentary migration of a drift.

4.4. Eastern Slope

On the eastern slope of the Derbent Basin, there are no such clear contourite features as are observed on its western and northern slopes and discussed above. At the base of the eastern slope (water depths 550–600 m), seismic profiles cross a depositional body (Figure 14) and extend across the slope for around 150 km. Their orientation is controlled by a specific slope morphology that is likely affected by a deep fault. The thickness of the body (down to the KT reflector) is about 50 m, while the upper part of the seismic section is characterized by a distinct undulation of reflectors appearing in a hummocky surface of the body. Reflector undulation is also slightly expressed below the KT. The mounded depositional feature is separated from the slope by a moat-like asymmetrical feature with a depth of 30 m and a width up to 2 km. In a big stretch, we can assume that this is a separated drift (see Section 5.2 of this paper) with a corresponding erosion moat; however, the orientation perpendicular to the contour along-slope flow is unusual for contour structures. Below the top of this depositional body, the lower stratified sequence is crumpled into small symmetrical wavy features (Figure 14).

Another atypical characteristic is box-shaped rootless fold features on the eastern slope of the Derbent Basin (Figure 15). Previously, such features were interpreted here as exogenic–gravitational folds or creep deformation produced by the plastic flow of poorly consolidated sediments under the influence of gravitational forces [9].

5. Discussion

The processes controlling recent sedimentation in closed water basins are similar in some cases, while differing significantly in others. For example, high-resolution seismic studies in Lake Saint-Jean (Québec, Canada) revealed the presence of sedimentary structures controlled by currents, which owe their origin to the movement of air masses [47,48]. In particular, they refer to the formation of sedimentary drifts and intense erosion within the shelf, which are caused by wind-related hydrodynamics. The peculiarity of these processes, according to the authors, is that they manifest themselves in the central part of the lake at depths below the wave base. The authors note that the change in the lake hydrodynamics is associated with the post-glacial processes that took place 8.5 cal. ka BP. An analysis of modern sedimentation in the tropical Lake Ossa and its relation to climatic changes, morphology and hydrology of this large water reservoir in West Africa is the subject of the article by Giresse et al. [49]. Of interest for us in this work is the fact that the hydrological features of the lake are related to the Sanaga River. Another example of studying the relationship between hydrodynamic processes and sedimentation is the Lake Superior sediment study. The description of samples and their seismostratigraphic identification served as the basis for the conclusion that the distribution of surface sediments was related to the glacial and post-glacial evolution of the lake [50,51].

Sedimentation processes in the Middle Caspian Sea are quite complicated. On the one hand, there are the turbidity currents in the western part, where the high fluvial input and deposition rate of unconsolidated sediments provide slope instability, while seismic activity triggers gravity flows and structures caused by local earthquakes [52]. We consider the results of the hyperpycnal flows as well. On the other hand, there are strong bottom currents forming a giant counterclockwise gyre that embraces the central part of the sea [33,53]. The activity of these processes has resulted in a wide range of erosional and depositional features, as illustrated above.

All these accumulative features fall into two groups: sediment waves (types 1, 2, 3) and large elongated sediment mounds (drifts). Erosional moats and channels are related to some of these sedimentary accumulative features. In general, the collected high-resolution seismic reflection data suggest the existence of contourite accumulative and erosive forms around the Derbent Basin in the Middle Caspian Sea. Below, we consider the possibility of combining them within the framework of regional physiography and oceanographic processes.

Possible accumulative and erosive sedimentary contourite features were first identified on the northern and especially western slopes of the Derbent Basin [5,41]. Its southern and eastern slopes are much less studied, but sedimentary features similar to the contourite ones appear to be observed there as well [6]. Such features over all slopes are illustrated below sequentially, in order to then consider their possible association with a single contourite sedimentary complex, according to the contourite paradigm [2].

5.1. Genesis of Wavy Features

In the study area, three major types of sediment waves (SW) were distinguished: SW Type 1, mixed waves [40,42] that come from an environment which favored both turbidite and contourite processes; SW Type 2, formed by turbidity flows, including those on channel meanders; and SW Type 3, sediment waves of contourite origin formed by bottom currents.

SW Type 1. The sparker seismic profiles on the western slope of the Derbent Basin show strong undulating reflectors (Figures 4 and 5), which recall the complex history of transgressions and regressions in the Caspian Sea. The most peculiar features are spectacular seafloor and subsurface undulations (Figures 4 and 5). They are interpreted as sediment waves but no syn- or post-sedimentary gravity deformation within the Quaternary sediments or creep was possible [40,43]. Along the western slope, the numerous rivers from the adjacent Caucasus represent the main regional sediment source. The sediment wave field is only 30–40 km from the coast, and the supply of terrigenous sediments is abundant here. Such waves seem to comply with these conditions of migrating sediment waves and are believed to have formed from sedimentary material transported and deposited by cyclic high density turbidity currents [54–56]. In particular, the thickness of the sediment wave sequences decreases naturally downstream, that is, downslope because the volume of splayed sediment is reduced away from its source. However, oceanographic data indicate that active bottom currents strongly influenced the seafloor, controlling the morphology of the sediment waves (see erosion on Figure 5B). The erosion exists just nearby an active branch of the bottom current [33]; the vertical profile of water is shown on Figure 16A1 (ellipsoids mark current maximum zones). The diagram in Figure 16C1 demonstrates the relation between wavelength and water depth. The form of graph of this function is sinusoidal. Its maximum extremes are for greater wavelength, and on seismic data (Figure 16B1) they correlate to areas of modern erosion. Previous work interprets this erosion places caused by bottom current activity [40]. Lithological data show coarse sediments on both sides of the waves, which together with the oblique orientation of wave crests and two-directional migration (upslope, i.e., upstream the turbidity flows, and along slope, upstream the bottom currents) appear to suggest the mixed origin of these sediment waves.

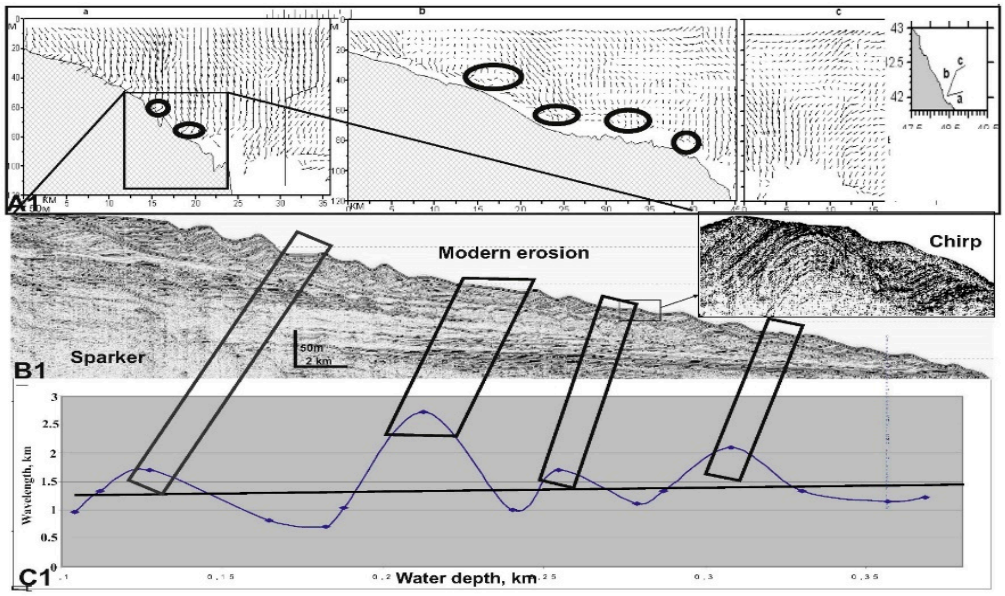

Figure 16. Modern erosion and resuspension on upper part of the western slope (sediment waves field, Figure 5A). Wavelength—Water depth relation, sinusoid, and linear trend (**C1**) correlated with hydrophysical profile (**A1**) and sparker section (**B1**) (seismic from Figure 5A). Circles for current branches. Details of modern erosion are shown on Chirp data (sweep seismoacoustic signal, inset).

SW Type 2. Several fields of wavy features exist on the Mangyshlak Sill (Figures 7 and 17). These features are interpreted as channel levee sediment waves migrating toward the channel. The sediment waves on levees are believed to have formed by classic outspill on channel meanders [57].

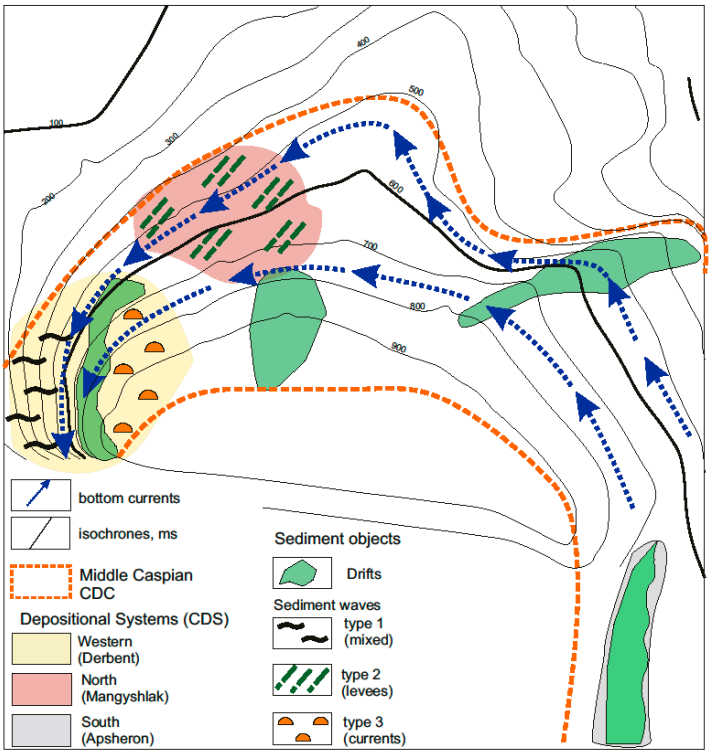

Figure 17. Contourite deposits (sediment waves and contourite drifts), contourite depositional complex (CDC) and contourite depositional systems (CDS) in the Middle Caspian Sea. Arrows show large circumcaspian current (Modified from [6]).

An atypical characteristic is the box-shaped rootless fold features on the eastern slope of the Derbent Basin (Figure 15). They were interpreted as exogenic–gravitational folds or creep deformation produced by the plastic flow of poorly consolidated sediments under the influence of gravitational forces [9].

SW Type 3. The vast field of undulations is located between the western and northern slopes, where the western slope turns eastward to the Mangyshlak Sill (Figure 8). Unlike sediment waves on the western slope (Figures 4 and 5), there appears to be no pronounced migration of crest and no symmetry in crest steep here (Figure 9). Such patterns together with the absence of alluvial sediments supply suppose that the waves here seem to be "contouritic" genesis. The "corner" looks like a natural "trap" for the bottom current. Its flow is activated by material coming from the channel system and is hampered by a sharp change of topography from the fairly gentle slope of the Mangyshlak Sill to the steep Derbent slope. As a result, the current throws off the "excess weight" of sediments and forms the sediment waves. After this, the current follows the topography, turns to the south, and erodes the western slope.

5.2. Contourite Sedimentary Drifts

Classic contourite sedimentary drifts are found in the Derbent Basin near the base of each of its slopes. At the base of the western slope, at water depths from 450 to 750 m, there are three large accumulative sedimentary bodies ~70 m thick with inconsistent internal reflectors (Figures 6 and 17). The overall geometry and visual seismic reflection pattern (down-current elongation, extensive regional unconformities, broadly lenticular, upward-convex seismic units, extensive sub-parallel moderate to low amplitude reflectors typically with gradual changes between seismic facies [58]), allow us to attribute these three depositional mounds to elongated mounded drift. It is believed that such drifts are formed as a result of the migration and aggradation of sediments [59,60]. The sedimentation rate of around 25 cm/kyr was calculated for these bodies [33]. According to seismic data, they are typical separated drifts [3]. As three of these individual separated drifts partly overlap each other, they build up a giant mounded elongate drift that extends along the western slope of the Derbent Basin.

The large lenticular accumulative sedimentary body is observed at water depths from 670 to 720 m nearby the Mangyshlak Sill (Figure 11). The body looks like a large, detached drift. Its complicated seismic reflection pattern appears to evidence the existence of several internal small detached and plastered drifts. This large contourite drift is located opposite the mouths of manifold channels that intersect the slope (Figure 10). Typical buried channel levels are found inside this body (Figure 11A), while the spectacular channel-looking feature is at its top. In general, this indicates that the formation of this body was strongly affected by turbidity currents from the adjacent channel system. Lenticular seismic units with distinct channels represent deposits of gravity flows. We suggest a contourite origin of the under- and overlying deposits with slightly undulating, parallel reflectors. However, in the bottom relief, the drift is complicated by a channel-looking structure, implying the modern activity of gravity flows in this area and the interplay between down-slope and along-slope processes. The studied depositional body is interpreted as a mixed turbidite-contourite system.

Two contourite drifts seem to have formed in the southern slope of the Derbent Basin off the Apsheron Sill. The southern one is an upward convex lenticular gently sloped depositional body located in upper slope at a water depth of ~350 m (Figure 12). It is characterized by the pinching-out upslope of the internal reflectors and local unconformities within the thin-layered strata. We interpret the unconformities as a lateral migration of the sedimentary features, which could be plastered drift. The northern contourite feature is divided by the obvious fault into two segments which together form typical fault-controlled drift (Figure 13). The acoustical transparent anomalies indicative of gas escape are widely distributed in the Caspian Sea [44,61]. Similar weak acoustic anomalies are observed in this area (Figure 13B).

The high-resolution seismic reflection profiles intersect a coupled erosive moat and depositional body at the base of the eastern slope of the Derbent Basin (Figure 14). The across-slope orientation of the depositional body is interpreted to have been caused by the interplay between regional bottom topography and specific circulation pattern. Seismic and bathymetric data suggest a deep fault modifying the slope morphology. The rapid change in slope trend makes the bottom current turn sharply to the east. This results in a significant increase in current intensity. Bottom circulation here is also complicated due to a thermo-cline upwelling gyre [33]. The Caspian Sea is filled with salty sea water. This is due to the connection in the recent geological past (Pleistocene) of the Caspian Sea with the Black Sea and the Mediterranean Sea through the Manich and Bosporus Straits, respectively, whereas other large, enclosed lakes such as the Great Lakes and Baikal are freshwater. It is the thermohaline structure of the waters that determines their density with which the formation of bottom currents is connected. Lack of data concerning this erosion-depositional system allows only preliminary interpretation, where the depositional body is initially interpreted as a separated drift, while a local depression detaching the drift likely represents an erosive moat.

5.3. Middle Caspian Contourite Depositional Complex

The association of various individual depositional drifts and related moats form part of a contourite depositional system (CDS) [3,62]. In turn, distinct but connected CDS within the same water mass are considered a contourite depositional complex (CDC). According to this idea, the whole investigated area in the Middle Caspian Sea with various contourite drifts and fields of sediment waves seems to contain several CDS.

One CDS is probably located in the western part of the Middle Caspian Sea, covering the western continental slope and rise and extending deeper in the adjacent basin (Figure 17). The most prominent feature in this CDS is elongated mounded and separated drift near the base of the continental slope; other prominent features here are sediment waves on the slope and in the basin. Another CDS located in the northern part near the Mangyshlak Sill and the adjacent basin is related to a widespread channel system with which expressive contourite drift and sediment waves are associated. In general, both these contourite sedimentary systems (western and northern) are apparently parts of a more extensive contourite sedimentary complex spanning the respective parts of the Middle Caspian Sea. The contourite drifts revealed on the southern slope and adjacent basin near the Apsheron Sill suggest that CDS exists here too. However, we currently do not have enough high-resolution seismic reflection data to be certain. Regarding the eastern slope, available high-resolution seismic reflection data show no CDS at this time.

The synthesis of contouritic deposits in the Middle Caspian Sea evidence that their position coincides with the general route of the circumcaspian current (Figure 17). In this case, a large single contourite depositional complex related to this circumcaspian current would exist along the whole continental rise of central part of the Middle Caspian Sea at a depth range from 250 to 720 m. This CDC should integrate both contourite depositional systems revealed in its western and north-western parts, the proposed CDS in the southern part and confidently expected CDS in the eastern part (Figure 17).

According to analysis and stratigraphic interpretation of seismic profile formation of the Middle Caspian, the contourite depositional complex started at least 250 kyr ago (since the Khvalinian transgression). To have a better idea of the existence of this circular contourite depositional complex, purposeful seismic reflection surveys should be carried out in the Middle Caspian Sea.

Contourite drifts can develop accumulations with important seal potential for trapping hydrocarbons; however, the subject of academic studies based on traditional shallow penetration high-resolution seismic 2D data and sea-floor piston coring are not contourites associated with oil-bearing reservoirs [63]. The modern contourites and turbidites of the Caspian Sea contain large amount of organic plant matter, which can subsequently become a source of hydrocarbons under the appropriate temperature-pressure regime. Our

high-resolution seismic reflection profiles do not penetrate deep enough to answer the question: do these modern sedimentary systems act as possible analogues for any of the subsurface hydrocarbon discoveries in the region? It is also necessary to have an idea of the paleoenvironment and paleowater circulation in the Caspian Sea during the accumulation of ancient sedimentary oil and gas-bearing sediments. Therefore, while any conclusions about such an analogy are premature, perhaps a dedicated study in the future will answer this question.

5.4. Geohazards

The Caspian Sea is a large hydrocarbon basin of great value, with its most remarkable geohazards, along with shallow gas accumulation within sediments and regional seismicity, being the bottom water circulation and its sediment transport. That is, both downslope gravity mass transport and transport by turbidity and contour currents. Every natural process is responsible for a geological seafloor feature, which can be seen on seismic sections.

The hydrodynamic regime of the Middle Caspian Sea is a very complicated one; velocities of near-bottom currents are high (15–100 cm/s) and have a different direction here [33]. The most dangerous appear to be submarine pipelines, which stretch along all sediment forms and pathways of various natural processes. Thus, it is very important to know the slope stability and sediment transport pattern.

The downslope gravity and turbidity flow on the western slope, which causes erosion of the seafloor and intensive sediment input, are treacherous for submarine pipelines and could cause ruptures. The SES seismic profiling data indicate that the processes of such turbidite sedimentation in the studied area of the western slope of the Derbent Basin are probably accompanied by active underwater slumping. This fact should be considered in the designation of engineering structures within the petroliferous Yalama-Samur structure (Figure 18). This issue is especially important because of the substantial thickness (more than 200 m) deposits west of the studied area [10,11].

Another danger, related to the canyon-channel system in Mangyshlak Sill, is turbidity sediment waves on their levees, which are indicators of active hydrodynamics. One more such danger relates to contourite sediment waves in the Derbent Basin near all its slopes. Thus, any pipeline construction will face issues, making it necessary to obtain more data regarding the current picture and the bottom relief. It should be noted that the gravitational folding and faulting on the northern slope of the Derbent Basin were most intense precisely in the Holocene [11].

The investigation of high-pressure fluids including shallow gas and gas hydrate is important for the risk assessment of marine geohazards and for localizing conventional and unconventional hydrocarbon reservoirs [64]. Gas-related processes may cause geohazards or may be considered a natural source of energy in the near future. For example, pipelines often have to wind their way through pockmarks fields, adding to the cost of construction. Furthermore, for other structures, they may represent a significant hindrance and may severely limit the freedom of the areal use of construction [65].

As a result of the analysis of our seismic profiles, a map of geohazards in the Middle Caspian was compiled, and the most pertinent geo-hazard threats in each region were diagnosed [40], to which we made additions and reworked (Figure 18). They should be taken into consideration when designing, building, and operating submarine constructions for the oil and gas industry in order to prevent potential natural hazards and reduce their consequences.

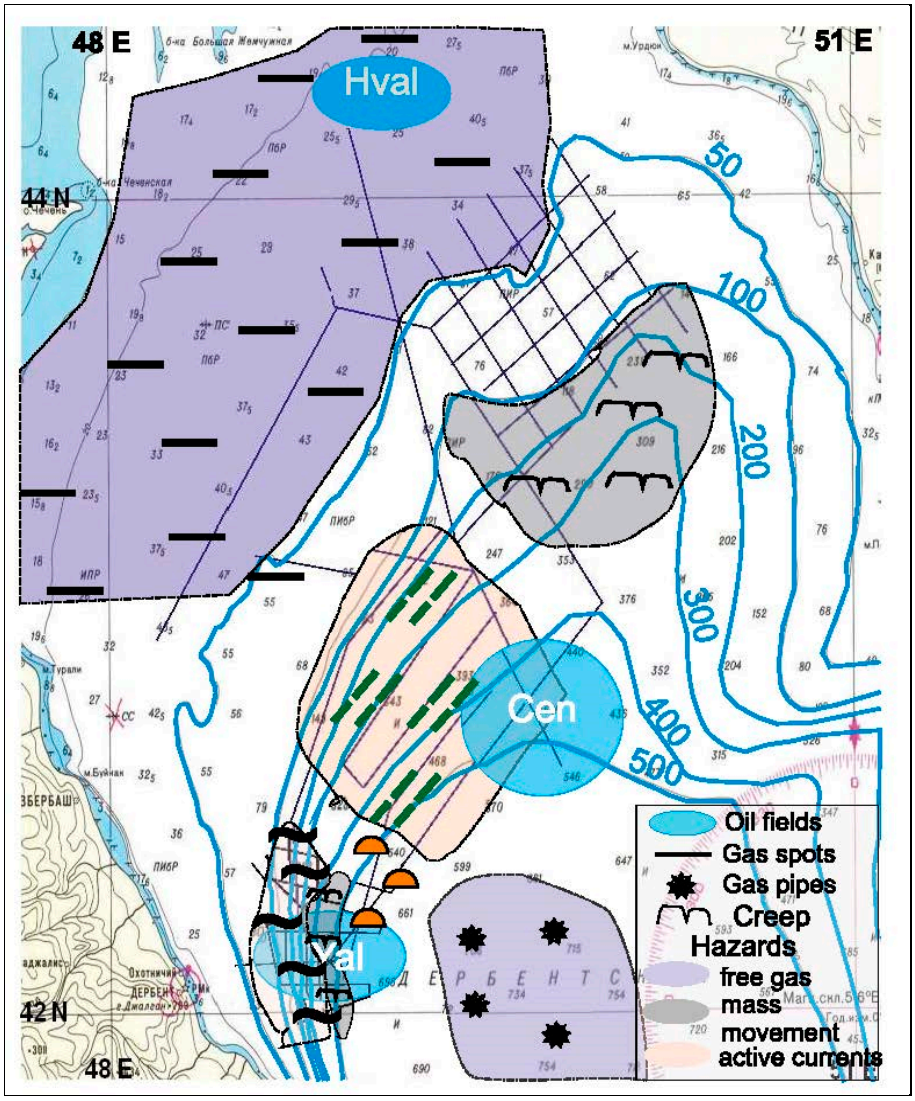

Figure 18. Map of sedimentary features and geohazards. Bathimetry in meters. Oil fields: Hval—Khvalynskoe, Cen—Centralnaya, Yal—Yalama-Samur. For sediment features legend see Figure 17.

6. Conclusions

The Caspian Sea is an important region for the investigation of lake contourites. This was confirmed by a wide range of contourite erosional and depositional features revealed in the Middle Caspian Sea for the first time. Contourite drifts, sediment waves and moats build a large contourite depositional complex covering a major part of the Middle Caspian Sea. This complex is formed by the strong counterclockwise gyre of bottom currents and was developed during the last 250 kyr (at least). In the north, the complex is affected by turbidity currents, while the interplay between along-slope and down-slope sedimentation processes resulted in the formation of mixed depositional features, such as sediment waves and sediment mounds.

The modern contourites and turbidites of the Caspian Sea contain a large amount of organic plant matter, which could subsequently become a source of hydrocarbons under the appropriate temperature–pressure regime. Our high-resolution seismic reflection profiles do not penetrate deep enough to answer the following question: do these modern sedimentary systems act as possible analogues for any of the subsurface hydrocarbon discoveries in the region? It is also necessary to have an idea of the paleoenviroment and paleowater circulation in the Caspian Sea during the accumulation of ancient sedimentary

oil- and gas-bearing sediments. Therefore, while any conclusions about such an analogy are premature; perhaps a dedicated study in the future will answer this question.

These results should be taken into consideration when designing, building, and operating submarine constructions for the oil and gas industry to prevent potential natural hazards and reduce their consequences.

Author Contributions: Conceptualization, methodology, V.Y., O.L.; validation, V.Y., O.L., V.P.; investigation, V.Y., O.L., V.P.; writing—original draft preparation, V.Y., O.L., V.P.; writing—review and editing, V.Y., O.L., V.P.; discussion, interpretation of results and conclusions, all authors; visualization (preparation of figures), O.L., V.P.; supervision, V.Y., O.L.; project administration, V.Y., O.L. All authors have read and agreed to the published version of the manuscript.

Funding: Financial support for this research was partially provided by Instituto Potosino de Investigación Científica y Tecnológica, A.C. The research was funded by the state assignment of IO RAS: FMWE-2021-0005.

Institutional Review Board Statement: Not applicable.

Informed Consent Statement: Not applicable.

Data Availability Statement: The original data are property of Shirshov Institute of Oceanology, it could be available to third parts after consideration of official request.

Acknowledgments: The authors are grateful to Graham Tippett for the editing the English version. The authors are grateful to three anonymous reviewers and to the editor for valuable observations that have improved the manuscript.

Conflicts of Interest: The authors declare no conflict of interest.

References

1. Duarte, C.S.L.; Viana, A.R. Santos Drift System: Stratigraphic organization and implications for late Cenozoic palaeocirculation in the Santos Basin, SW Atlantic Ocean. In *Economic and Palaeoceanographic Significance of Contourite Deposits*; Viana, A.R., Rebesco, M., Eds.; Geological Society, Special Publications: London, UK, 2007; Volume 276, pp. 171–198.
2. Rebesco, M.; Camerlenghi, A. (Eds.) *Contourites*; Elsevier: Amsterdam, The Netherlands, 2008; p. 666.
3. Rebesco, M.; Hernández-Molina, F.J.; Van Rooij, D.; Wåhlin, A. Contourites and associated sediments controlled by deep-water circulation processes: State-of-the-art and future considerations. *Mar. Geol.* **2014**, *352*, 111–154. [CrossRef]
4. Ceramicola, S.; Rebesco, M.; De Batist, M.; Khlystov, O. Seismic evidence of small-scale lacustrine drifts in Lake Baikal (Russia). *Mar. Geophys. Res.* **2001**, *22*, 445–464. [CrossRef]
5. Levchenko, O.V.; Roslyakov, A.G.; Polyakov, A.S.; Zverev, A.S.; Merklin, L.R. New data about sedimentary waves on western continental slope of the Caspian Sea. *Dokl. Earth Sci.* **2008**, *420*, 537–542. [CrossRef]
6. Levchenko, O.; Putans, V.; Borisov, D. Contourites in the Middle Caspian Sea? In Proceedings of the 2nd Deep-Water Circulation Congress, Ghent, Belgium, 10–12 September 2014; pp. 65–66. Available online: https://www.vliz.be/imisdocs/publications/264048.pdf (accessed on 10 May 2022).
7. Levchenko, O.V.; Putans, V.A.; Borisov, D.G. Contourites in the Derbent Basin, Caspian Sea (Geophysical Data). *Dokl. Earth Sci.* **2018**, *482*, 1239–1243. [CrossRef]
8. Putans, V.A.; Levchenko, O.V.; Borisov, D.V. Circum Middle Caspian Contourite Depositional Complex. In *Abstracts of the VIII Simposio MIA15*; Universidad de Málaga: Malaga, Spain, 2015.
9. Maev, E.G. Exogenous Folding in Quaternary Deposits of the Continental Slope of the Caspian Sea. *Dokl. Earth Sci.* **1999**, *365*, 323–325.
10. Verzhbitsky, V.E.; Levchenko, O.V.; Lobkovsky, L.I. New Data on Quaternary Processes of Underwater Slumping on the Western Slope of the Derbent Basin (Caspian Sea). *Dokl. Earth Sci.* **2007**, *416*, 1085–1089. [CrossRef]
11. Verzhbitsky, V.E.; Lobkovsky, L.I.; Roslyakov, A.G.; Merklin, L.R.; Polyakov, A.S.; Levchenko, O.V.; Kovachev, S.A.; Zverev, A.S.; Garagash, I.A.; Mar, G.N. Slump Structures in Quaternary Slope Sediments of the Northern Derbent Basin (Caspian Sea). *Oceanology* **2009**, *49*, 396–404. [CrossRef]
12. Mir, N. *English Version of Explanatory Notes of International Tectonic Map of the Caspian Sea Region*; Scale 1:2, 500,000; Khain, V.Y., Bogdanov, N.A., Eds.; Russian Academy of Science: Moscow, Russia, 2005.
13. Hinds, D.J.; Aliyeva, E.; Allen, M.B.; Davies, C.E.; Kroonenberg, S.B.; Simmons, M.D.; Vincent, S.J. Sedimentation in a diascharge dominated fluvial-lacustrine system: The Neogene Productive Series of the South Caspian Basin, Azerbaijan. *Mar. Pet. Geol.* **2004**, *20*, 613–638. [CrossRef]

14. Leroy, S.A.G.; Lahijani, H.A.; Cretaux, J.-F.; Aladin, N.V.; Plotnikov, I.S. Past and current changes in the largest lake of the World: The Caspian Sea. In *Large Asian Lakes in a Changing World. Springer Water*; Mischke, S., Ed.; Springer: Cham, Switzerland, 2020; pp. 65–107. [CrossRef]
15. Arpe, K.; Bengtsson, L.; Golitsyn, G.S.; Mokhov, I.I.; Semenov, V.A.; Sporyshev, P.V. Connection between Caspian Sea level variability and ENSO. *Geophys. Res. Lett.* **2000**, *27*, 2693–2696. [CrossRef]
16. Lebedev, L.I. Structure of upper part of sedimentary cover according to geoacoustical profiling. In *Caspian Sea: Geology and Oil and Gas Resources*; Nauka: Moscow, Russia, 1987; pp. 105–114.
17. Kostyanoy, A.G.; Kosarev, A.N. *The Caspian Sea Environment*; Springer: Berlin, Germany, 2005.
18. Ivanova, T.P.; Trifonov, V.G. Seismotectonics and modern regime of Caspian Sea level fluctuations. *Geotectonics* **2002**, *2*, 27–42.
19. Yutsis, V.V.; Kalinin, V.V. Pliocene-Quaternary geodynamics of the Apsheron shelf of the Caspian Sea revealed by geological-geophysical data. In Proceedings of the Geodynamic Basis of Prognostication of Oil and Gas, Moscow, Russia, 6–8 September 1988.
20. Leonov, Y.G.; Antipov, M.P.; Bobylova, E.E.; Volozh, Y.A.; Lavrushin, Y.A.; Spiridonova, E.A. *Geological History of Quaternary Sedimentary Basins within Caspian Region during Last 700,000 Years: Sedimentation Its Water Regimen and Geodynamics Events [Comments to "Map of Quaternary (Neo Pleistocene) Sediments within Caspian Area with Elements of Paleogeography", Scale 1:2,500,000]*; Scientific World: Moscow, Russia, 2005; Volume 3. (In Russian)
21. Chen, J.L.; Pekker, T.; Wilson, C.R.; Tapley, B.D.; Kostianoy, A.G.; Cretaux, J.-F.; Safarov, E.S. Long-term Caspian Sea level change. *Geophys. Res. Lett.* **2017**, *44*, 6993–7001. [CrossRef]
22. Golubov, B.N.; Ismagilov, D.F. Pipe-looking structures under the Northern Caspian fluid regime. In Proceedings of the All-Russia Conference of Oil and Gas Genesis, Moscow, Russia, 15–18 April 2003; pp. 78–80.
23. Kosarev, A.N.; Kostyanoy, A.G.; Zonn, I.S. Kara-Bogas-Gol Bay: Physical and chemical evolution. *Aquat. Geochem.* **2009**, *15*, 223–236. [CrossRef]
24. Leonov, Y.G.; Antipov, M.P.; Volozh, Y.A. Geological Aspects of Caspian Sea Level Fluctuations. In *Global Changes of Environment*; Siberian RAS: Novosibirsk, Russia, 1988; pp. 30–57.
25. Kravchishina, M.D.; Novigatskii, A.N.; Politova, N.V.; Zernova, V.V.; Mosharov, S.A.; Dara, O.M.; Klyuvitkin, A.A. Studying the biogenic and abiogenic parts of suspended particulate matter in the Volga delta during spring flood of May 2008. *Water Resour.* **2013**, *40*, 143–156. [CrossRef]
26. Kozina, N.V.; Putas, V.A.; Zhdan, M.I. Elaboration of sediment transport pathways by integrated interpretation of geological and high-resolution seismoacoustic data (Caspian Sea). In *Proceedings of the Dialogue between Contourite and Oceanology Processes International Workshop*; Hull, UK, 28–26 January 2013, 2013; p. 34.
27. Lahijani, H.; Abbasian, H.; Naderi-Beni, A.; Leroy, S.A.G.; Haghani, S.; Habibi, P.; Hosseindustn, M.; Shahkeremi, S.; Yeganeh, S.; Zandinasab, Z.; et al. Sediment distribution pattern of South Caspian Sea: Possible hydroclimatic implications. *Can. J. Earth Sci.* **2018**, *56*, 637–653. [CrossRef]
28. Kosarev, A.N. *Hydrology of the Caspian and Aral Seas*; Moscow State University: Moscow, Russia, 1975; p. 372.
29. Terziev, F.S.; Kosarev, A.N.; Kerimov, A.A. *Hydrometeorology and Hydrochemistry of Seas*; Caspian Sea, Hydrometeorological Conditions, Gidrometeoizdat: St. Petersburg, Russia, 1992; Volume 6. (In Russian)
30. Ghaffari, P.; Lahijani, H.A.K.; Azizpour, J. Snapshot observation of the physical structure and stratufucation in deep-water of the South Caspian Sea (western part). *Ocean Sci.* **2010**, *6*, 877–885. [CrossRef]
31. Sapozhnikov, V.V.; Mordasova, N.V.; Metreveli, M.P. Transformations in the Caspian Sea ecosystem under the fall and rise of the sea level. *Oceanology* **2010**, *50*, 488–497. [CrossRef]
32. Glumov, I.F.; Malovitsky, Y.P.; Novikov, A.A.; Senin, B.V. *Regional Geology and Oil and Gas Content of the Caspian Sea*; Nedra: Moscow, Russia, 2004; p. 342. (In Russian)
33. Ambrosimov, A.K.; Ambrosimov, E.C.; Libina, N.V. Dynamic structure of currents near western slope of the Derbent Basin in the Caspian Sea. *Eng. Phys.* **2010**, *10*, 31–45.
34. Ambrosimov, A.K.; Klyuvitkin, A.A.; Lisitsyn, A.P. Season variations of currents over the western slope of the middle Caspian bed. *Water Resour.* **2018**, *45*, 685–694. [CrossRef]
35. Kroonenberg, S.B.; Badyukova, E.N.; Storms, J.E.A.; Ignatov, E.I.; Kasimov, N.S. A full sea-level cycle in sixty-five years: Barrier dynamics along Caspian shores. *Sediment. Geol.* **2000**, *134*, 257–274. [CrossRef]
36. Hoogendoorn, R.M.; Boels, J.F.; Kroonenberg, S.B.; Simmons, M.D.; Aliycva, E.; Babazadeh, A.D.; Huseynov, D. Development of the Kura delta, Azerbaijan; a record of Holocene Caspian Sea level changes. *Mar. Geol.* **2005**, *222–223*, 359–380. [CrossRef]
37. Klige, R.K.; Myagkov, M.S. Changes in the water regime of the Caspian Sea. *GeoJournal* **1992**, *27*, 299–307. [CrossRef]
38. Meshcherskaya, A. Analysis of global climatic characteristics in relation to Caspian Sea Level. In *TA-CIS/Caspian Environmental Programme, Report WLF*; Centre for Water Level Change: Almaty, Kazakhstan, 2001; p. 63. (In Russian)
39. Kroonenberg, S.B.; Abdurakhmanov, G.M.; Badyukova, E.N.; van der Borg, K.; Kalashnikov, A.; Kasimov, N.S.; Rychagov, G.I.; Svitoch, A.A.; Vonhof, H.B.; Wesselingh, F.P. Solar-forced 2600 BP and Little Ice Age Highstands of the Caspian Sea. *Methods Ecol. Res. South Russ. Ecol. Dev.* **2008**, *173–174*, 12–21. [CrossRef]
40. Putans, V.A.; Merklin, L.R.; Levchenko, O.V. Sediment waves and other forms as evidence of geohazards (Caspian Sea). *Int. J. Offshore Polar Eng.* **2010**, *20*, 1–4.
41. Putans, V.A. Sediment waves: Geohazard or geofeature? *Hydro Int.* **2013**, *10*, 25–29.

42. Levchenko, O.V.; Roslyakov, A.G. Cyclic sediment waves on western slope of the Caspian Sea as possible indicators of main transgressive/regressive events. *Quat. Int.* **2010**, *225*, 210–220. [CrossRef]
43. Levchenko, O.V.; Gainanov, V.G.; Merklin, L.R.; Polyakov, A.S.; Roslyakov, A.G. New data about seismic stratigraphy and sedimentological proscesses over western continental slope of the Middle Caspian Sea. *Dokl. Earth Sci.* **2006**, *355*, 671–673.
44. Gerivani, H.; Putans, V.A.; Merklin, L.R.; Modarres, M.H. Characteristics of features formed by gas hydrate and free gas in the continental slope and abyssal plain of the Middle Caspian Sea. *Mar. Georesourc. Geotechnol.* **2020**, *39*, 419–430. [CrossRef]
45. Andreassen, K.; Hubbard, A.; Winsborrow, M.; Patton, H.; Vadakkepuliyambatta, S.; Plaza-Faverola, A.; Gudlaugsson, E.; Serov, P.; Deryabin, A.; Mattingsdal, R. Massive blow-out craters formed by hydrate-controlled methane expulsion from the Arctic seafloor. *Science* **2017**, *356*, 948–953. [CrossRef]
46. Nixon, F.C.; Chand, S.; Thorsnes, T.; Bjarnadóttir, L.R. A modified gas hydrate-geomorphological model for a new discovery of enigmatic craters and seabed mounds in the Central Barents Sea, Norway. *Geo-Mar. Lett.* **2019**, *39*, 191–203. [CrossRef]
47. Nutz, A.; Schuster, M.; Ghienne, J.-F.; Roquin, C.; Hay, M.B.; Retif, F.; Certain, R.; Robin, N.; Raynal, O.; Cousineau, P.A.; et al. Current-controlled Sedimentary Features into Lake Saint-Jean (Québec, Canada): A Record of Wind-driven Processes? In Proceedings of the AGU Fall Meeting, San Francisco, CA, USA, 15–19 December 2014.
48. Nutz, A.; Ghienne, J.-F.; Schuster, M.; Certain, R.; Robin, N.; Roquin, C.; Raynal, O.; Bouchette, F.; Duringer, P.; Cousineau, P.A. Seismic-stratigraphic record of a deglaciation sequence: From the marine Laflamme Gulf to Lake Saint-Jean (late Quaternary, Québec, Canada). *BOREAS* **2014**, *43*, 309–329. [CrossRef]
49. Giressea, P.; Maley, J.; Kossoni, A. Sedimentary environmental changes and millennial climatic variability in a tropical shallow lake (Lake Ossa, Cameroon) during the Holocene. *Palaeogeogr. Palaeoclimatol. Palaeoecol.* **2005**, *218*, 257–285. [CrossRef]
50. Thomas, R.L.; Dell, C.I. Sediments of Lake Superior. *J. Great Lakes Res.* **1978**, *4*, 264–275. [CrossRef]
51. Tonello, M.S.; Hebner, T.S.; Sterner, R.W. Geochemistry and mineralogy of southwestern Lake Superior sediments with an emphasis on phosphorus lability. *J. Soils Sediments* **2020**, *20*, 1060–1073. [CrossRef]
52. Putans, V.A.; Merklin, L.R.; Zelenin, E.A. Signs of modern tectonic events in Late-Quaternary sediments of middle Caspian. *Adv. Curr. Nat. Sci.* **2018**, *4*, 139–144. [CrossRef]
53. Ambrosimov, A.K.; Klyuvitkin, A.A.; Kozina, N.V.; Kravchishina, M.D.; Libina, N.V.; Filippov, A.S.; Artamonova, K.V.; Torgunova, N.I.; Baranov, V.I.; Pol'kin, V.V. Complex studies of the Caspian Sea system during the 41st cruise of the R/V Rift. *Oceanology* **2014**, *54*, 671–676. [CrossRef]
54. Lee, H.J.; Syvitski, J.P.M.; Parker, G.; Orange, D.; Locat, J.; Hutton, E.W.H.; Imran, J. Distinguishing sediments waves from slope failure deposits: Field examples, including the "Humboldt slide", and modeling results. *Mar. Geol.* **2002**, *192*, 79–104. [CrossRef]
55. Normark, W.R.; Piper, D.J.W.; Posamentier, H.; Pirmez, C.; Migeon, S. Variability in form and growth of sediment waves on turbidity channel levees. *Mar. Geol.* **2002**, *192*, 23–58. [CrossRef]
56. Cattaneo, A.; Correggiari, A.; Marsset, T.; Thomas, Y.; Marsset, B.; Trincardi, F. Seafloor undulation pattern on the Adriatic shelf and comparison to deep-water sediment waves. *Mar. Geol.* **2004**, *213*, 121–148. [CrossRef]
57. Wynn, R.B.; Piper, D.J.; Gee, W.; Martin, J.R. Generation and migration of coarse-grained sediment waves in turbidity current channels and channel lobe transition zones. *Mar. Geol.* **2002**, *192*, 59–78. [CrossRef]
58. Wynn, R.B.; Stow, D.A.V. Classification and characterization of deep-water sediment waves. *Mar. Geol.* **2002**, *192*, 7–22. [CrossRef]
59. Hernandez-Molina, F.J.; Stow, D.A.V. Continental slope contourites. In *Contourites: Developments in Sedimentology 60*; Rebesco, M., Camerlenghi, A., Eds.; Elsevier: Amsterdam, The Netherlands, 2008; pp. 379–408.
60. Rebesco, M. Contourites. In *Encyclopedia of Geology*; Selley, R.C., Cocks, L.R.M., Plimer, I.R., Eds.; Elsevier: Oxford, UK, 2005; pp. 513–527.
61. Ivanov, A.Y.; Golubov, B.N.; Zatyagalova, V.V. On oil and gas potential and subsoil fluid discharge in southern part of Caspian Sea by satellite geolocation data. *Earth Satell. Res.* **2007**, *2*, 62–81.
62. Hernandez-Molina, F.J.; Paterlini, M.; Violante, R.; Marshall, P.; de Isasi, M.; Samoza, L.; Rebesco, M. Contourite depositional system on the Argentine slope: An exceptional record of the influence of Antarctic water masses. *Geology* **2009**, *37*, 507–510. [CrossRef]
63. Viana, A.R.; Almeida, J.R.W.; Nunes, M.C.V.; Bulhoes, E.M. The economic importance of contourites. In *Economic and Palaeoceanographic Significance of Contourite Deposits*; Viana, A.R., Rebesco, M., Eds.; Geological Society, Special Publications: London, UK, 2007; Volume 276, pp. 1–23.
64. Roy, S.; Hovland, M.; Braathen, A. Evidence of fluid seepage in Grønfjorden, Spitsbergen: Implications from an integrated acoustic study of seafloor morphology, marine sediments and tectonics. *Mar. Geol.* **2016**, *380*, 67–78. [CrossRef]
65. Hovland, M.; Gardner, J.V.; Judd, A.G. The significance of pockmarks to understanding fluid flow processes and geohazards. *Geofluids* **2002**, *2*, 127–136. [CrossRef]